Chapter 2.1

Satellite Ocean Color Sensor Design Concepts and Performance Requirements

Charles R. McClain,* **Gerhard Meister, Bryan Monosmith**

NASA Goddard Space Flight Center, Greenbelt, MD, USA

*Corresponding author: Email: charles.r.mcclain@nasa.gov

Chapter Outline

1. INTRODUCTION

In late 1978, the National Aeronautics and Space Administration (NASA) launched the Nimbus-7 satellite with the Coastal Zone Color Scanner (CZCS) and several other sensors, all of which provided major advances in Earth remote sensing. The inspiration for the CZCS is usually attributed to a article in *Science* by Clarke et al. [1] who demonstrated that large changes in open ocean spectral reflectance are correlated to chlorophyll-a concentrations. Chlorophyll-a is the primary photosynthetic pigment in green plants (marine and terrestrial) and is used in estimating primary production, i.e., the amount of carbon fixed into organic matter during photosynthesis. Thus, accurate estimates of global and regional primary production are key to studies of the earth's carbon cycle. Because the investigators used an airborne radiometer, they were able to demonstrate the increased radiance contribution of the atmosphere with altitude that would be a major issue for spaceborne measurements.

Since 1978, there has been much progress in satellite ocean color remote sensing such that the technique is well established and is used for climate change science and routine operational environmental monitoring. Also, the science objectives and accompanying methodologies have expanded and evolved through a succession of global missions, e.g., the Ocean Color and Temperature Sensor (OCTS), the Sea-viewing Wide Field-of-view Sensor (SeaWiFS), the Moderate Resolution Imaging Spectroradiometer (MODIS), the Medium Resolution Imaging Spectrometer (MERIS), and the Global Imager (GLI). With each advance in science objectives, new and more stringent requirements for sensor capabilities (e.g., spectral coverage) and performance (e.g., signal-to-noise ratio, SNR) are established. The CZCS had four bands for chlorophyll and aerosol corrections. The Ocean Color Imager (OCI) recommended for the NASA Pre-Aerosol, Cloud, and ocean Ecosystems (PACE) mission includes 5 nm hyperspectral coverage from 350 to 800 nm with three additional discrete near infrared (NIR) and shortwave infrared (SWIR) ocean aerosol correction bands. Also, to avoid drift in sensor sensitivity from being interpreted as environmental change, climate change research requires rigorous monitoring of sensor stability. For SeaWiFS, monthly lunar imaging accurately tracked stability at an accuracy of $\sim 0.1\%$ that allowed the data to be used for climate studies [2]. It is now acknowledged by the international community that

future missions and sensor designs need to accommodate lunar calibrations. An overview of ocean color remote sensing and a review of the progress made in ocean color remote sensing and the variety of research applications derived from global satellite ocean color data are provided in Refs [3] and [4], respectively.

The purpose of this chapter is to discuss the design options for ocean color satellite radiometers, performance and testing criteria, and sensor components (optics, detectors, electronics, etc.) that must be integrated into an instrument concept. These ultimately dictate the quality and quantity of data that can be delivered as a trade against mission cost. Historically, science and sensor technology have advanced in a "leap-frog" manner in that sensor design requirements for a mission are defined many years before a sensor is launched and by the end of the mission, perhaps 15−20 years later, science applications and requirements are well beyond the capabilities of the sensor. Section 3 provides a summary of historical mission science objectives and sensor requirements. This progression is expected to continue in the future as long as sensor costs can be constrained to affordable levels and still allow the incorporation of new technologies without incurring unacceptable risk to mission success. The IOCCG[1] Report Number 13 [5] discusses future ocean biology mission Level-1 requirements in depth.

2. OCEAN COLOR MEASUREMENT FUNDAMENTALS AND RELATED SCIENCE OBJECTIVES

The basis of ocean color remote sensing lies primarily in the selective absorption of key pigments found in phytoplankton and other biogenic substances like colored dissolved organic matter (CDOM), but also in the scattering properties of some species like coccolithophores and particulates. Generally, as pigment concentrations increase, the ocean reflectance spectral slope "rotates" from negative to positive, i.e., from blue to red, as absorption suppresses the blue and scattering elevates the red (more pigment is associated with more particles). Water is highly transmissive in the blue, but highly absorbing in the red so that the ocean water-leaving radiance is derived from increasingly shallower depths with increasing wavelength. According to Pope and Fry [6], the greatest transmission is between 400 and 450 nm with the maximum being at 418 nm. One important point to make is that the chlorophyll-a and -b in vivo absorption peaks (440 and 470 nm, respectively [7]) coincide with the extraterrestrial solar spectrum peak around 450 nm as well as the maximal water transmission. Given that chlorophyll-a concentrations range from ~ 0.02 mg l^{-1} to over 200 mg l^{-1} (more than four orders of magnitude), the dynamic ranges of downwelling irradiance and, therefore, water-leaving radiance are greatest in the blue which is optimal for remote sensing of chlorophyll. Also,

---

1. Purpose and current membership of the International Ocean-Colour Coordinating Group (IOCCG) is provided at www. ioccg.org.

high water absorption in the NIR and SWIR means ocean reflectance is small and allows for estimation of top-of-the-atmosphere (TOA) aerosol radiance which must be subtracted along with atmospheric molecular scattering (Rayleigh radiance) in the estimation of the ocean reflectances at shorter wavelengths [8−10]. In Wang [9] and subsequent papers, MODIS SWIR bands at 1260, 1640, and 2130 were used for aerosol corrections over turbid waters having finite NIR ocean reflectance even though the SNRs of these bands are significantly lower than what would be desired, i.e., the bands were not designed for this purpose. The European Space Agency's Ocean and Land Colour Instrument (OLCI) will have a band at 1020 nm for this purpose.

Of course, there are complications. One is that CDOM absorption exponentially increases in the visible and ultraviolet (UV). At 440 nm, both chlorophyll-a and CDOM are highly absorbing. To separate the two constituents requires measurements at lower wavelengths, e.g., 360 nm. Historically, including UV bands below 410 nm in satellite ocean color sensors has proven to be a challenge for a number of reasons. SeaWiFS, MODIS, MERIS, and other sensors included bands around 410 nm, but with limited success for this application. To date, only one sensor, the GLI on Advanced Earth Observing Satellite-2 (ADEOS-2), included an ocean color band below 410 nm, i.e., a band at 380 nm (the follow-on sensor, the Second Generation Global Imager or SGLI also has a 380 nm band). The issues include sensor optical throughput and the rapidly decreasing solar irradiance in the UV that limit SNR, as well as relatively greater Rayleigh scattering atmospheric contributions.

Aside from chlorophyll-a and CDOM, other pigments with different absorption spectra may be useful in identifying the presence of key classes of phytoplankton or functional groups [11] and [12]. The identification of these pigments requires additional spectral bands than those of historical multispectral sensors like SeaWiFS, MODIS, and MERIS. For instance, bands at 495, 545, and 625 nm have been recommended for *Trichodesmium*, 655 nm for chlorophyll-b, 470 nm for carotenoids, and 620 nm for phycocyanin [5]. The approach applied in [12] is based on derivative analyses which require a continuous spectrum over the UV−visible domain, i.e., hyperspectral data. Also, the research community is moving to spectral inversion algorithms to estimate derived products [13], the accuracy of which improves with the number and range of the input wavelengths. The distinction between multispectral and hyperspectral is essentially that multispectral implies discrete bands at specific wavelengths while hyperspectral implies a continuous spectrum at a designated resolution, e.g., 5 nm.

Historically, multispectral ocean color sensors placed bands within atmospheric "windows" which are outside major gas (particularly O_2, O_3, NO_2, and water vapor) absorption bands when possible. However, gases like O_3 and NO_2 have absorption bands in the ocean color critical visible which are too broad to

avoid and require explicit corrections relying on other ancillary data sources for the global distributions of these gas concentrations. NO_2 absorbs in the UV and blue portions of the spectrum making corrections in bands between 340 and 490 nm essential, especially in coastal areas where pollution is high and water-leaving radiances are small [14]. O_3 has significant absorption in the green portion of the spectrum, around 555 nm (e.g., SeaWiFS) in particular, making accurate corrections necessary because of the sensitivity of bio-optical band ratio algorithms that use 555 nm in the denominator. However, O_3 absorption is nearly zero between 340 and 400 nm, but its absorption does increase rapidly at wavelengths below 340 nm. O_2 has a strong absorption band, the A-band, at 758–770 nm. The SeaWiFS 765 nm band straddled the A-band requiring a correction [15,16]. There are reasons for making A-band measurements that could be beneficial to ocean color atmospheric corrections such as estimation of aerosol plume heights [17], although, in their study, this application required aerosol optical depths >0.3 which exceeds the value normally allowed for valid ocean color retrievals. Finally, water vapor has strong absorption bands around 820, 940, 1125, 1375, and 1875 nm that broaden with wavelength. Water vapor also has a minor absorption band around 720 nm. There have also been recommendations for a thin cirrus cloud flag or correction using a 1380 nm band [18,19], but the necessity of the correction is not unanimous [20,21]. For continuous hyperspectral data spanning the UV–NIR as is being proposed for the NASA PACE mission, corrections for all these absorbing gases will be necessary. The hyperspectral data may allow inversion techniques to be used to estimate gas concentrations simultaneously, but this remains to be demonstrated.

While there are bio-optical signatures below 340 nm, atmospheric ozone effectively blocks any upwelling ocean radiance, at least at detectable levels for a satellite sensor. Other major problems in the UV are the rapid drop in the solar spectrum and increased atmospheric Rayleigh scattering (Rayleigh radiance is proportional to λ^{-4}) making the UV atmospheric radiance especially large compared to the relatively small ocean signals. For comparison, the Rayleigh radiance at 350 nm is about 16 times that at 700 nm. An additional consideration is that the Rayleigh radiance is highly polarized, the degree of polarization (DOP) being determined by the solar geometry with respect to the viewing geometry (Figure 1). In the visible domain, ocean upwelling radiances are no more than about 15% of the TOA radiance with the remaining 85% being largely Rayleigh radiance for clear ocean scenes. Therefore, if a sensor has a 5% sensitivity to polarization that is not characterized or corrected for and the scene or pixel has a Rayleigh radiance equaling 85% of the total radiance with a DOP of 70%, the estimated uncertainty or error is 0.05 * 0.85 * 0.70 or about 3% of the TOA radiance which translates to a $\sim$30% or greater error in water-leaving radiance estimates. For this reason, ocean color sensors need to be designed to minimize polarization sensitivity in order to minimize uncertainties in the on-orbit calibration and atmospheric
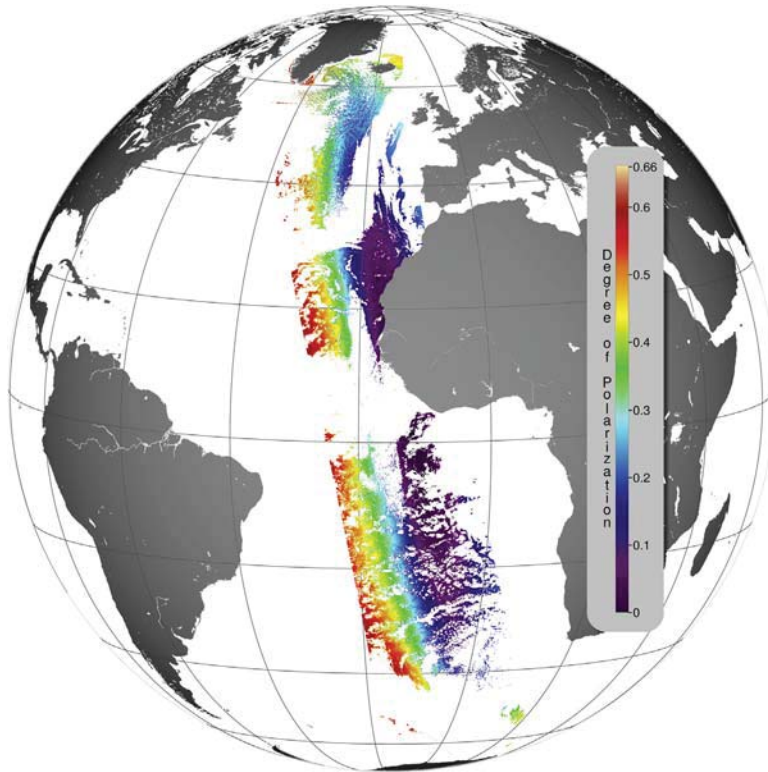
FIGURE 1 The degree of polarization (DOP) at 412 nm computed for a MODIS Aqua orbit on March 22, 2003. DOP $= (I_p - I_s)/(I_p + I_s)$ where I_p and I_s are the intensities of the parallel and perpendicular components of the polarized light, respectively. The range of values in the figure is $0-0.662$.

corrections. Because of the sensitivity of bio-optical algorithms for quantities like chlorophyll-a, accurate removal of atmospheric radiance (Rayleigh and aerosol) and high signal-to-noise performance are required. Also, another reason for measurements in the UV is the potential for identifying and correcting for absorbing aerosols at low optical thicknesses (e.g., less than 0.3 in the blue), a problem that has not been solved for heritage ocean color sensors.

Finally, a critical consideration in sensor design is the orbit and the temporal coverage desired. In the past, ocean color missions have been in low earth sunsynchronous orbits meaning that the satellite orbits the earth in essentially a fixed plane with the earth rotating under it such that the satellite passes over head at about the same local time each orbit. The overpass time for ocean color missions has been between 10:00 am and 2:00 pm in order to optimize solar illumination. Low solar zenith angles (high solar elevation) increase sunglint, so sensors like the CZCS and SeaWiFS had a tilt capability to minimize glint

contamination. Orbital altitudes for low earth orbits (LEO) have ranged from 705 km for SeaWiFS and MODIS to 955 km for the CZCS. The altitude affects the orbital period, the swath width for a given sensor view or scan angle range, and the sensor instantaneous field of view (IFOV) for a specified ground resolution. The orbital velocity and period can be calculated as.

$$v = (Gm_e/r)^{1/2} \tag{1}$$

$$T = 2\pi r^{3/2}(Gm_e)^{-1/2} \tag{2}$$

where G is the universal gravitational constant ($6.67 * 10^{-11}$ $\text{m}^3\text{Kg}^{-1}\text{s}^{-2}$), m_e is the earth's mass ($5.98 * 10^{24}$ kg), and r is the sum of the earth's radius ($6.37 * 10^6$ m) + the orbital altitude. For a 650 km orbit, $v \approx 7.5$ km/s and $T \approx 97$ min. The orbital velocity dictates many aspects of the design, e.g., the scan rate for sensors like SeaWiFS and MODIS. In the SeaWiFS design, the telescope rotated at ∼6 Hz to achieve the required 1.1 km ground resolution at nadir (with some overlap). At that rate of rotation, a time-delay-integration (TDI) scheme using four detectors was implemented to meet the SNR requirements, i.e., each detector sees the ground pixel at slightly different times and the signals are summed because a single detector would not accumulate an adequate number of photons over the sample integration or dwell time for each ground pixel to achieve the desired SNR. The benefit of LEO sun-synchronous orbits is that the entire global ocean can be routinely observed subject to cloud cover. The frequency of global coverage depends on the sensor swath width and orbital altitude. For example, a sensor having an FOV (also called field of regard) of ±60° with a 20° tilt at 650 km altitude, views the entire globe daily with no gaps between swaths, even at the equator.

Besides LEO, there are geostationary orbits where the spacecraft rotates with the earth so that the surface area viewed remains constant. Geostationary orbit altitudes are ∼36,000 km with the spacecraft usually positioned on the equator. Variations of geostationary orbits that allow the spacecraft to move north and south of the equator in a periodic fashion, e.g., seasonally, are possible. The advantage of geostationary orbits is frequent views daily, depending on the rapidity in which the sensor can collect the data, the area to be sampled, and the spacecraft transmission and ground station receiving data rates. Another advantage is that the sensor can "stare" at a scene for much longer than LEO, thereby improving SNR by offsetting the "distance-squared" decrease in photons received from a ground pixel. Staring can require jitter control to avoid ground resolution degradation and adds complexity and cost to the sensor. To date, the only geostationary ocean biology mission is the Korean Geostationary Ocean Color Imager (GOCI), although a follow-on mission has been approved. The IOCCG Report Number 12 [22] provides a detailed description of the science and sensor design considerations for a geostationary ocean color mission.

3. EVOLUTION OF SCIENCE OBJECTIVES AND SENSOR REQUIREMENTS

Sensor design and performance requirements are necessarily linked to the science objectives of the mission. Normally, a science traceability matrix (STM) is defined which provides (1) the scientific questions to be addressed, (2) the approaches to answering the questions using the satellite sensor data, complementary field data, modeling, etc., (3) the satellite geophysical data products, and (4) other mission requirements and activities that must be supported to ensure mission success. In outlining these, the sensor measurement requirements (e.g., spectral bands and SNR; [23]) must be specified as well. An STM for future ocean color missions is outlined in [5]. From a historical perspective, the science objectives have evolved dramatically from those of the CZCS. Table 1 provides a brief (and simplified) summary of how mission science objectives have expanded over time with the corresponding impacts on sensor design and complexity. Overall, the objectives have evolved from simply demonstrating that a useful pigment product could be estimated from space to measuring a variety of phytoplankton pigments, dissolved and particulate constituents, phytoplankton functional groups and physiological properties, and more.

Not only has the number of research products increased, each with spectral coverage requirements, but over time, algorithms have incorporated more spectral information, all of which expand the spectral coverage requirements. The CZCS band ratio algorithm [25] correlated ratios of 443/550 and 490/550 to pigment concentration (chlorophyll-a + phaeophytin) with a switch to the latter when the 443 nm water-leaving radiance dropped below a threshold value. O'Reilly et al. [26] used the sum of three band ratios to avoid discrete algorithm switching which generally produces discontinuities in the pigment distributions. One aspect of product development is the substantial lag between algorithm formulation and postlaunch product verification. Product verification requires substantial numbers of field samples for match-up comparisons with satellite estimates. Typically, only about 10−15% of the possible match-up samples pass quality control criteria, e.g., cloud cover [27]. Semianalytical models as discussed in [28] invert ocean reflectance spectra to estimate inherent optical properties (IOPs; absorption and scattering coefficients) and provide estimates of chlorophyll-a, but the inversion fidelity increases with the number of spectral reflectance wavelengths. Thus, as the research community moves to more sophisticated and accurate algorithms based on semianalytical models, spectral requirements are increasing as well as ocean reflectance spectral accuracy because these models are more sensitive to error than band-ratio algorithms, i.e., additional emphasis on sensor performance and calibration accuracy.

Overall, this progress has been the result of the research community constantly pushing beyond each sensor and mission's original science

TABLE 1 Chronological Sequence of Research Ocean Color Missions Illustrating the Evolution of Science Applications and Sensor Complexity (e.g., Number of Spectral Bands)

Sensor	Primary Ocean Science Objectives	Primary Bio-optical Data Products (Prelaunch)	Bio-optical Spectral Bands (nm)	Comments
CZCS (1978)	Feasibility of measuring chlorophyll-a (Chl-a) from space	Total pigment (Chl-a + phaeophytin), K(490)	3 bands: 443, 490, 550	• 670 nm band used for aerosol corrections. • 8-bit digitization • Noise equivalent radiance (NEΔL) at 443 nm: $0.21\ Wm^{-2}\ sr^{-1}\ \mu m^{-1}$
OCTS (1996) SeaWiFS (1997)	• Global net primary productivity (NPP) • Global Chl-a time series	Chl-a, K(490)	6 bands: 412, 443, 490, 510/520, 555, 670	• Bands at 765 and 865 nm included for aerosol corrections. • Solar diffusers added for on-orbit stability monitoring. • SeaWiFS monthly lunar maneuvers of stability monitoring • 10-bit digitization • NEΔL at 443 nm: 0.11 and $0.077\ Wm^{-2}\ sr^{-1}\ \mu m^{-1}$, respectively • NPP, CDOM, IOPs, calcite, particulate organic carbon (POC), photosynthetically available radiation (PAR) added after launch. 412 nm band inadequate for accurate separation of Chl-a and CDOM limiting accuracy of PP estimates based on Chl-a.

Continued

TABLE 1 Chronological Sequence of Research Ocean Color Missions Illustrating the Evolution of Science Applications and Sensor Complexity (e.g., Number of Spectral Bands)—cont'd

Sensor	Primary Ocean Science Objectives	Primary Bio-optical Data Products (Prelaunch)	Bio-optical Spectral Bands (nm)	Comments
MODIS (2000 & 2002)	• Global NPP • Global Chl-a time series • Fluorescence line height (FLH) applications	Chl-a, K(490), CDOM, FLH, calcite, IOPs	7 bands: 412, 443, 488, 531, 547, 668, 678	• 12-bit digitization • NEΔL at 443 nm: 0.032 Wm^{-2} sr^{-1} µm^{-1} • FLH found useful indicator of Fe limitation, but of limited use for Chl-a. • Spacecraft roll maneuvers approved postlaunch for lunar calibration. • Saturation of red and NIR bands over bright areas problematic for lunar calibration.
MERIS (2002)	• Global NPP • Global Chl-a time series • Coastal water quality evaluation (e.g., turbidity, red tides)	Chl-a, K(490), CDOM, FLH, total suspended matter (TSM)	9 bands: 412, 443, 490, 510, 560, 620, 665, 681, 709	• High resolution (300 m) for coastal applications • NEΔL at 443 nm: 0.025 Wm^{-2} sr^{-1} µm^{-1} • Additional bands for suspended sediment and red tides.

	Science objectives	Products	Bands	Notes
GLI (2002)	• Global NPP • Global Chl-a time series • Water quality (e.g., turbidity, red tides)	Chl-a, K(490), CDOM, FLH, TSM	13 bands: 380, 400, 412, 443, 460, 490, 520, 545, 565, 625, 666, 680, 710	• 380 and 400 nm added for improved separation of Chl-a and CDOM. • NEΔL at 443 nm: 0.054 Wm^{-2} sr^{-1} μm^{-1}
OCI (as discussed in IOCCG, 2012; see Table 2 in Section 4 below for details)	• Global NPP • Global Chl-a time series • Water quality • Marine carbon budget • Ecosystem structure (e.g., phytoplankton functional groups) • Particle properties (e.g., size distribution) • Phytoplankton physiological properties	Chl-a, K(490), CDOM, FLH, calcite, IOPs, NPP, POC, PAR, TSM, phytoplankton functional groups, particle size distributions, C:Chl ratio, fluorescent yield	19 bands: 350, 360, 385, 412, 425, 443, 460, 475, 490, 510, 532, 555, 583, 617, 640, 655, 665, 678, 710	• NASA PACE science definition team recommended hyperspectral coverage with 5 nm resolution from 350 to 800 nm, two SWIR (1260 and 1640 nm) bands for ocean color aerosol corrections over highly turbid water, a 900 nm band for water vapor corrections, no sensor saturation over clouds (high L_{max}) in any band, monthly full moon lunar calibrations and 14-bit digitization.

"Primary ocean science objectives" are not all-inclusive and have been paraphrased somewhat from what is stated in various mission documents. Similarly, "primary bio-optical data products" have been redefined or standardized. In both instances the purpose is to show commonality between missions and to reflect international efforts to converge on common products. Also, in most cases, the product suite was expanded in the post-launch phase as new algorithms were developed and data sets were shared and reprocessed by different groups. The visible infrared imaging radiometer suite (VIIRS), SGLI, and OLCI are not included for the sake of space, but all three have fewer bio-optical bands (5, 6, and 11, respectively) than GLI (13) and provide products similar to previous sensors with commensurate capabilities. OLCI will be the first ocean color sensor with a 1024 nm band for aerosol corrections over turbid water. The CZCS NEΔL at 443 nm values are taken from IOCCG report number 1 [24].

objectives after launch, thereby laying the groundwork for the next mission. Column 5 of Table 1 includes some of the additional products developed in the postlaunch phase of the missions, most of which were incorporated into the product suites of other subsequent missions.

4. PERFORMANCE PARAMETERS AND SPECIFICATIONS

The performance specifications laid out in this chapter follow the suggestions presented in [5], which are the consensus as agreed upon by representatives from the following space agencies (in alphabetical order): Center national d'etudes spatiales (CNES), European Space Agency (ESA), Japan Aerospace Exploration Agency (JAXA), Korean Aerospace Research Institute (KARI), NASA, National Oceanic and Atmospheric Administration (NOAA). The report was also reviewed by the IOCCG which has representation from essentially all space agencies with an active interest in ocean color research. The specifications are also very similar to the sensor requirements for an advanced ocean color radiometer developed by the NASA Goddard Space Flight Center Ocean Ecology Laboratory [23]. This section includes specific recommendations for the verification of the requirements.

4.1 Spectral Coverage and Dynamic Range

An overview of the wavelengths needed to address the ocean color science issues discussed in [5] is given in Table 2. Usually, it is not required to match the exact wavelengths of Table 2. However, for all bands, the center wavelength should be known to within ∼0.1 nm because processing algorithms are tuned to the band centers and relative spectral response (RSR) functions. The NASA PACE Science Definition Team requirements for the OCI are outlined in [29].

Table 2 also provides the typical radiances (L_{typ}), the nominal bandwidth (the bandwidth used for SNR calculation), as well as the *minimum* required SNR. L_{typ} is generally specified as the most frequent clear sky radiance over the open ocean. The L_{typ} at the wavelengths common to the SeaWiFS and MODIS sensors were derived from on-orbit data (MODIS values were scaled to the SeaWiFS values). The L_{typ} of the remaining bands were calculated using the Thuillier solar irradiance (F_0) values [30] and interpolations or extrapolations of the L_{typ}/F_0 ratios of the SeaWiFS/MODIS bands. The maximum radiance L_{max} is provided in Table 2 as well to help define the dynamic range. It was calculated using an albedo of 1.1 and 0° incidence angle to simulate the brightest case of a white cloud for an orbit with an equator overpass time of around noon. The SNRs in Table 2 are comparable to those of SeaWiFS. Sensors like MODIS had much higher SNRs (∼factor of 2 or more at the listed L_{typ}'s which should be the goal of future sensors).

The RSR needs to be measured for each band and each sensor element (e.g., mirror, camera, and detector). The out-of-band (OOB) response should

TABLE 2 Multispectral Band Centers, Bandwidths, Typical TOA Clear Sky Ocean Radiances (L_{typ}), Saturation Radiances (L_{max}), and *Minimum* SNRs at L_{typ}

λ	$\Delta\lambda$	L_{typ}	L_{max}	L_{min}	L_{high}	SNR (min)
350	15	74.6	356			300
360	15	72.2	376			1000
385	15	61.1	381			1000
412	15	78.6	602	50	125	1000
425	15	69.5	585			1000
443	15	70.2	664	42	101	1000
460	15	68.3	724			1000
475	15	61.9	722			1000
490	15	53.1	686	32	78	1000
510	15	45.8	663	28	66	1000
532	15	39.2	651			1000
555	15	33.9	643	19	52	1000
583	15	28.1	624			1000
617	15	21.9	582			1000
640	10	19.0	564			1000
655	15	16.7	535			1000
665	10	16.0	536	10	38	1000
678	10	14.5	519			1400
710	15	11.9	489			1000
748	10	9.3	447			600
765	40	8.3	430	3.8	19	600
820	15	5.9	393			600
865	40	4.5	333	2.2	16	600
1245	20	0.88	158	0.2	5	250
1640	40	0.29	82	0.08	2	180
2135	50	0.08	22	0.02	0.8	100

Radiance units are W/m² μm str. SNR is to be measured at L_{typ}. L_{min} and L_{high} are TOA radiance ranges for valid ocean color retrievals derived from a SeaWiFS global one-day data set for the respective SeaWiFS bands after removing the 0.5% highest and 0.5% lowest radiances. These values need to be derived for the remaining bands in the future. Adjustments may be necessary for sensors with different solar and viewing geometries. This table is taken from IOCCG report number 13 [5].

be less than 1% of the total response (where OOB region is defined as those wavelengths where RSR < 0.01; in-band region are wavelengths RSR ≥ 0.01). The characterization is typically achieved by shining light of well-defined wavelength and small bandwidth (e.g., <1 nm) into the sensor. The spectral sampling resolution is ideally related to the response: the larger the response, the finer the sampling. The spectral sampling range needs to be broad enough to capture all significant energy contributions. In the case of a silicon-based detector, this could be 340−1000 nm, for example. For the OOB measurements, the light intensity is increased because of the low expected response. For the in-band measurements, the light intensity is decreased to avoid saturation. The center wavelength λ_c can be calculated from the RSR measurements with the full-width-half-maximum value and should be known with an accuracy of <0.5 nm.

The RSR should be characterized for every sensor element or at least for a representative subset. Variations of the center wavelength for different sensor elements should be less than 0.5 nm. For cross-track scanning sensors, it is generally sufficient to characterize the RSR at one view angle such as nadir, especially if an instrument model has shown that the dependence of the RSR on scan angle is negligible. The RSR should be characterized, as much as possible, involving the complete optical path.

Depending on the instrument design, an on-orbit spectral calibration approach may be required. It is generally accepted that such an approach is not required for filter-based instruments such as SeaWiFS and MODIS. For MODIS, it was demonstrated using an on-board spectral calibration device that the on-orbit spectral change was negligible [31]. However, for instruments such as MERIS an on-orbit spectral calibration approach is required because the dispersion from a grating is very sensitive to alignment changes which may occur, e.g., during launch. MERIS used a doped solar diffuser as well as absorption lines (solar and atmospheric) to determine its wavelength calibration [32].

4.2 Coverage and Spatial Resolution

At large sensor and solar zenith angles, the radiances contributed from the atmosphere become very large relative to the water-leaving radiances, which limits the useful solar and sensor zenith angle range for ocean color products [33]. For SeaWiFS and MODIS, 60° is the maximum sensor zenith angle that is used for level-3 (L3, spatially and/or temporally averaged or binned) data. For SeaWiFS, this translates to a maximum scan angle that is used of about 45° (because of the SeaWiFS tilt). Because MODIS is not tilted, its maximum scan angle used for L3 data binning is about 50° (less than 60° because of the Earth curvature). Another drawback to wide swaths and LEOs is the range of solar and sensor zenith angles which requires an accurate ocean bidirectional reflectance function (BRDF) correction. Experience from

SeaWiFS, MODIS, and MERIS show that reasonably accurate ocean color products can be derived for solar zenith angles $\leq \sim 70-75°$ and sensor zenith angles $\leq \sim 60°$ [5]. For global ocean color applications, a spatial resolution of 1 km at nadir has proven to be sufficient. For coastal and estuarine waters, a higher spatial resolution of $50-300$ m is desirable. Global coverage is improved with sensor tilting to minimize sunglint. According to Gregg and Patt [34], a tilted sensor can obtain 20% more coverage than an untilted sensor for a noontime orbit. Such a mechanism should be considered for any ocean color sensor.

For most science questions it is not sufficient to have a measurement at one point in time, but the measurements are required over a certain period of time (e.g., to study the seasonal variation of an ocean color product). Cloud coverage strongly reduces the number of valid retrievals, such that in many areas of the world (e.g., equatorial regions) with a revisit time of every other day there are locations with no valid ocean observations even over a week's time. Other examples are the arctic and Antarctic regions, where the revisit time is even higher due to the convergence of LEO orbits at the poles [35].

4.3 Radiometric Uncertainty

The IOCCG Report Number 10 [33] states that a goal of 0.5% for the accuracy of the TOA radiance at 443 nm is required to achieve a water-leaving radiance accuracy of 5% (at 443 nm) and an accuracy of the chlorophyll product of $\sim 30\%$ (see also [36]). Ideally, the required uncertainties should be defined for each science question. The ocean color community has accepted the method of vicarious calibration [37]. In practice, this means the initial prelaunch calibration is adjusted by the vicarious calibration, and the focus of the calibration effort shifts to the trending of the radiometric gains and the characterization of artifacts like spectral response changes, polarization, etc.

The accuracy goal of about 0.5% for the TOA signal is very challenging. Assuming error sources are uncorrelated, the total error is estimated by taking the square root of the sum of the squares of all individual uncertainty components (such as polarization, linearity, straylight, etc.). This requires the uncertainty of each individual component to be much smaller than 0.5%, preferably less than 0.2%.

There are two separate phases of the radiometer characterization: prelaunch and on-orbit. The prelaunch characterization is very extensive and includes as many aspects of the instrument as possible, whereas the on-orbit characterization is usually restricted to the measurement of the radiometric gain and the SNR, and possibly trending of the spectral responsivity and polarization. The testing protocols and procedures should be mature and vetted with the science community well before the start of the prelaunch characterization phase, in particular.

4.3.1 Prelaunch Absolute Radiance-Based Radiometric Calibration

The absolute radiometric calibration of the instrument is achieved by letting the sensor measure a calibrated light source. The radiance level of the light source should be SI (International System of Units) traceable to standards from national metrology institutes such as the National Institute of Standards and Technology in the United States. Spherical integrating spheres (SIS) are a popular light source, because their spectral output can be easily traced to standards, and they can achieve a high level of spatial uniformity at their exit aperture. Note that for nonscanning instruments such as MERIS, calibration of the complete FOV of the sensor can only be covered using an SIS by scanning the sensor's FOV across the aperture of the SIS, increasing significantly the uncertainty. The spheres are often illuminated by light from tungsten lamps, and a large number of lamps (placed at different positions in the sphere), in conjunction with the scattering inside the sphere (which is coated on the inside with a diffuse, highly reflective material) assures a high degree of spatial uniformity of the light output. The actual non-uniformity of both the output aperture and the back of the sphere need to be characterized (in the sensor's geometric configuration—pupil location and FOV) to reduce the errors. The multiple scattering inside the sphere leads to a very low DOP of the radiance exiting the SIS, the goal should be a DOP of less than 0.2%. After the light output of the SIS has been calibrated, it needs to be monitored (e.g., by sensors internal to the sphere) to ensure that the SIS radiance does not change from the time of the sphere calibration to the time of the radiometer calibration.

It may seem unnecessary to define a prelaunch radiance uncertainty requirement for sensors like MODIS or MERIS, whose ocean color products do not use the prelaunch gain. However, many of the prelaunch characterization tests (e.g., straylight, saturation, etc.) require an instrument gain to calculate the radiance, and therefore such a requirement is justified. The requirement for SeaWiFS and MODIS of 5% was relatively high, and modern technology can achieve better accuracies.

4.3.2 Prelaunch Absolute Reflectance-Based Radiometric Calibration

The reflectance calibration of an instrument applies to instruments that use a solar diffuser as their main on-orbit calibration source. The BRDF of the solar diffuser needs to be determined. As defined by Nicodemus et al. [38], the BRDF describes the absolute reflectance of a surface, as well as the dependence of the reflectance on incidence and view angles. These measurements need to be made so that all combinations of angles that are expected on-orbit are bracketed, with an angular resolution of better than 5°. The absolute uncertainty for the reflectance measurements should be better than 1%, and the

relative uncertainty at different angles with respect to each other should be ∼0.2%. If a device like a solar diffuser screen is used to avoid sensor saturation (e.g., MODIS), the characterization measurements should be done with the screen in place to determine the combined effect. An analysis of the MODIS on-orbit calibration measurements revealed a significant detector dependency of the vignetting (reduction in brightness) function [39] that was not measured prelaunch.

4.3.3 Relative Radiometric Calibration

The two previous sections described uncertainty goals for the absolute calibration. The calibration requirements of different sensor elements relative to each other (e.g., half-angle mirror sides for SeaWiFS, detectors or cameras for MERIS) need to be even tighter. The reason is that very small relative calibration inaccuracies for adjacent sensor elements are easily identifiable in images of ocean color products as stripes, which reduce the confidence of the user community in the overall product quality and is detrimental to the detection of spatial features in the level-2 (L2, derived products like ocean reflectance and chlorophyll-a) data. A SIS can provide a spatially homogeneous light field that can be used for relative calibration measurements. The gains of detector elements should be calibrated with an uncertainty relative to each other of ∼0.2%.

4.4 SNR and Quantization

The minimum SNR requirements are given in Table 2. They are the result of studies for the Aerosol, Cloud, Ecosystems (ACE; a NASA decadal survey mission in formulation) mission that were adopted by the PACE SDT. For the bands from 360 to 710 nm, the SNR requirements were derived from simulations using a semianalytical ocean color model [40], varying the spectral marine remote sensing reflectance and assessing the impact on biogeochemical variables. The 350 nm band is primarily for absorbing aerosol detection, so the SNR requirement (300) is lower than for other bands. The value of 1400 for the 678 nm band was derived from an analysis of MODIS retrievals of the fluorescence line height, which is a very small signal. The NIR and SWIR values were derived from a study of the sensitivity of the reflectance inversion bio-optical model to noise in atmospheric correction algorithms [8,9].

A 14-bit resolution is sufficient for most ocean color applications even when bright cloud radiance levels are included in the dynamic range. The requirements for quantization depend strongly on the radiance level and the sensitivity of the ocean reflectance to a particular ocean constituent: a very high degree of quantization is required at radiances typical of ocean scenes, but at higher radiance levels (e.g., over clouds and over land) a reduced degree of quantization is acceptable. This was achieved in the SeaWiFS instrument

with a bilinear gain (see the SeaWiFS description in the appendix). Generally, ocean color sensors have multiple gain modes where the gain is set via command (e.g., the CZCS) or using automatic gain switching (e.g., the Visible Infrared Imaging Radiometer Suite, VIIRS). However, different gain modes add considerable complexity to the sensor design, characterization and on-orbit calibration, and are generally not recommended now that 14-bit flight qualified analog-to-digital converters (ADC) are available. The main reason is that many on-orbit calibration or validation methods (e.g., lunar measurements or deep convective cloud analysis) operate at radiance levels higher than the typical clear sky ocean radiances. For bilinear gains or different gain modes, results obtained from these methods need additional analysis before they can be applied to the lower radiance levels, increasing the total uncertainty.

The instrument SNR is calculated using the noise of a single detector element when viewing a constant light source. The SNR must be determined for each band at L_{typ} (see Table 2). A SIS with a spatially homogenous output is often used for this test. Obviously, an excellent (and well-characterized) short-term temporal stability of the SIS light output is crucial for this test. Additionally, the SNR should be determined at various light levels within the dynamic range. This is often done in conjunction with the dynamic range test, and leads to a reduction in schedule and cost associated with sensor characterization.

4.5 Polarization

Circular polarization of the TOA signal is very low [41] and, therefore, does not need to be considered during sensor characterization. The degree of *linear* polarization of the TOA signal over the ocean can be up to 70% (44; Figure 1). This is not a problem for a sensor without polarization sensitivity. On the other hand, a sensor like MODIS/Aqua, with a polarization sensitivity of up to 5.4%, may produce radiance errors of up to 2.7% if the TOA signal is 50% polarized. Sensors like MERIS and SeaWiFS used polarization scramblers to reduce the instrument polarization sensitivity to low levels (SeaWiFS: about 0.3% or less, MERIS: less than 0.1% in the blue, $\sim 0.2\%$ in the NIR) and carry the residual polarization sensitivity as an uncertainty without modifying the measured radiances. Sensors with significant polarization sensitivity like MODIS need a correction to the TOA measured radiances using the sensor prelaunch polarization characterization data and radiative transfer model [41]. An incorrect polarization correction can lead to large regional and seasonal biases [42]. Thus, it is important to accurately characterize instrument polarization sensitivity.

One proven polarization characterization method is to use a SIS with low DOP, and to place a linear polarizer sheet (with well characterized polarization characteristics) between the SIS and the sensor. This method was used to characterize the polarization sensitivity of VIIRS. The polarizer sheet must

be rotated 180° (or preferably 360°, to confirm that the results 0−180° agree with the results from 180−360°), taking measurements with the sensor at intervals of about every 15°. These measurements must be obtained such that all scan angles (or the desired FOV) are covered. In many cases, this requires repeating the measurement sequence with different orientations of the sensor relative to the SIS. The overall goal should be to characterize the sensor polarization sensitivity with an uncertainty of about 0.2% [29].

4.6 Additional Characterization Requirements

Straylight refers to optical processes within the sensor, such as ghosts and optical scatter, and should be reduced as much as possible. Therefore, straylight must be a consideration early in the design process as it can seriously degrade data quality and straylight sources can be very difficult to isolate during testing. However, straylight is part of any optical sensor and can be minimized using baffling, special black paints, antireflection coatings on optics, etc. In the vicinity of strong radiance gradients, straylight effects often exceed the accuracy goal of 0.5%. Straylight can be particularly prominent in the vicinity of bright objects like clouds adjacent to relatively dark ocean areas and can seriously reduce global ocean coverage. As an example, in the case of MODIS Aqua, the masking of pixels due to straylight from clouds leads to a data loss of about 50% of all L2 ocean pixels for a given day [43]. If properly characterized prior to launch, straylight corrections can be made (e.g., SeaWiFS [44]) to recover some of the data.

Due to space limitations, only the sensor requirements most relevant to ocean color products have been discussed above. As for most Earth remote sensing sensors, the following items need to be characterized as well:

1. Linearity of the counts to radiance conversion
2. Temperature dependence
3. Dark current (offset) characterization
4. Spectral registration (or band coregistration, i.e., overlap of the footprint of different bands)
5. Pointing accuracy and knowledge (for geolocation purposes)
6. Modulation Transfer Function
7. IFOV

Additionally, every sensor needs comprehensive instrument models, e.g., throughput models for SNR estimation and ray trace models for component specification, straylight avoidance and alignment. Component, e.g., mirrors, lens, dichroics, gratings, detectors, and depolarizers, characteristics need to be tested and verified. Such models are essential in predicting performance in the design phase, in evaluating system performance during the characterization phase, and diagnosing problems on-orbit.

4.7 On-Board Calibration Systems

For space-based ocean color remote sensing, four different calibration approaches have been used historically:

- Lamps (e.g., CZCS, MODIS)
- Lunar observations (e.g., SeaWiFS, MODIS)
- Solar diffuser (e.g., MERIS, MODIS)
- Earth observations (e.g., MODIS)

Due to the high predictability of the lunar irradiance, the moon is an excellent calibration source. The main limitation of the moon is its small size relative to the instrument FOV. Lunar calibrations are described in a separate chapter (2.2).

On-orbit calibration with light bulbs has been only moderately successful (at best) in the past, because the brightness variation of a lamp over time is often larger than the ocean color radiometric stability requirements. Monitoring lamp output with photodiodes is necessary, but adds complexity. Lamp sources should only be considered for specific calibration subtasks (like spectral calibration, linearity, short term monitoring), not for absolute calibration or long-term trending [36].

Solar diffusers are a well-established approach for on-orbit calibration. The most common type is a reflective solar diffuser (e.g., MERIS, MODIS). Transmissive solar diffusers (e.g., GOCI) have been used, but much less frequently. For some instruments, they cover the full FOV (e.g., MERIS). The most commonly used material is space grade Spectralon. The main challenge regarding solar diffusers is to determine the reflectance change on-orbit. There are two main approaches to overcome this challenge:

a. The use of two solar diffusers, one of which is exposed to sunlight very infrequently (e.g., only every 3 months) to limit its reflectance degradation. The other diffuser is used for the more frequent calibration measurements. The ratio of the ocean color sensor measurements of the two solar diffusers is used to determine the reflectance degradation of the more frequently used solar diffuser. Additionally, by calculating the degradation as a function of exposure time for the more frequently used solar diffuser, the expected degradation of the less frequently solar diffuser can be calculated. This degradation can then be used in a correction algorithm. Note that for MERIS, the degradation of the less frequently used solar diffuser was negligible (less than 0.2% over the first 7 years; [45]).

b. The use of a solar diffuser stability monitor (SDSM). The SDSM on MODIS is a ratioing radiometer that successively views the solar diffuser and the sun. A screen is needed in the optical path between the SDSM detector and the sun, because the sun is so much brighter than the light reflected off the solar diffuser. Characterizing the vignetting function of this screen has been a challenge for the MODIS instruments [46]. An

additional potential problem is that the SDSM necessarily views the solar diffuser at a different angle than the MODIS instrument, and is therefore not able to capture any change in the relative BRDF of the solar diffuser. This is only a minor concern for small changes in solar diffuser reflectance, but the MODIS/Terra solar diffuser reflectance as measured by the SDSM has declined by about 50%. A similar degradation is expected for the solar diffuser used for VIIRS on the Suomi National Polar-orbiting Partnership project (US) mission. Limiting the solar exposure of the solar diffuser reduces the degradation of its reflectance and, therefore, this should be a design goal. MODIS achieves this goal by employing a door (unfortunately, this door has stopped working properly for MODIS/Terra) whereas MERIS moves the solar diffuser into a protected area. The solar diffuser on VIIRS is only protected by a screen, not a door, so it receives solar radiation every orbit. Also, the diffuser faces the velocity vector which increases its degradation. Therefore, its solar diffuser reflectance has degraded much faster than for MODIS or MERIS [47].

The MODIS ocean bands have a limited dynamic range. Therefore, it was necessary to reduce the illumination of the solar diffuser for the calibration of the MODIS ocean bands. This was achieved by a screen that transmits about 8% of the incoming light from the sun (via pinholes). The characterization of the vignetting function of this screen did not accurately capture the MODIS detector to detector differences seen on-orbit [39]. If possible, this source of radiometric uncertainty should be eliminated by choosing a dynamic range for the sensor that does not require a solar diffuser screen.

Using earth view data (e.g., ocean observations) is a common approach for ocean color sensors to adjust the absolute calibration of the sensor by one constant factor per spectral band ("vicarious calibration" [37]). For the case of MODIS/Terra, the standard calibration methods did not produce reasonable ocean color products, even after vicarious calibration. Because of the serious degradation of the MODIS/Terra mirror (e.g., reflectivity and polarization attributes), the SeaWiFS time series of global ocean products were used to provide time-dependent corrections to the MODIS/Terra standard calibration by modifying the scan angle dependence of the radiometric gains and the polarization sensitivity tables [48]. Although the approach was rather effective, it relies on the existence of reliable concurrent ocean color products from another global sensor, and therefore it should not be considered for sensors that claim to derive independent climate data records.

5. SENSOR ENGINEERING

The usual approach to defining a satellite sensor and scoping a mission (cost, facilities, etc.) is to formulate an STM as discussed in Section 4. In this section, some of the sensor engineering considerations are presented. Ocean
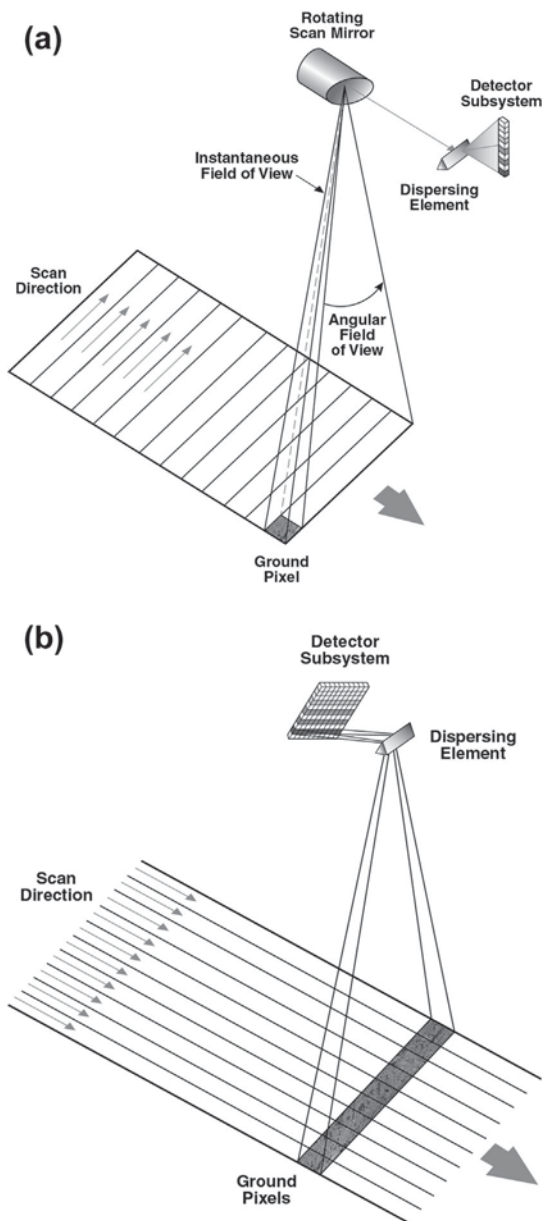
FIGURE 2 (a) Conceptual whiskbroom design and (b) conceptual pushbroom design. The large arrow on the right of each is the spacecraft ground track direction of motion. In panels (a) and (b), "dispersing element" can be a system of dichroic beam splitters and bandpass filters as in most multispectral instruments to date like SeaWiFS and MODIS or a prism or grating (e.g., MERIS). Whiskbroom designs include SeaWiFS and MODIS. In the case of SeaWiFS, each rotation of the telescope produced a single ground "swath" in the cross-track direction. Because MODIS had

10 detectors on each ocean color band focal plane aligned in the along track direction, a single rotation of the mirror produced 10 ground swaths in the cross-track direction. In (b), the 2D detector system has one dimension for spatial sampling corresponding to the along track line of ground pixels in the "scan direction" which is actually the satellite track direction as there is no mechanical scan. The other detector subsystem dimension is spectral. For a pushbroom design, the width of the swath can be increased by adding cameras or increasing the number of detectors in the spatial dimension.

color sensor design and fabrication requires the expertise of a broad range of engineering disciplines including the following: optical, mechanical, electro-mechanical, electrical, detector systems, thermal, contamination, quality assurance, calibration and characterization metrology, system integration and testing, and software development. Also, knowledge of the behavior and compatibility of all materials in a space environment is critical, e.g., outgassing and solder joints. All disciplines must work collaboratively because of the interdependencies of various design requirements and constraints. For instance, the optical, mechanical, and electro-mechanical design teams need to collectively ensure all optical elements (mirrors, lens, dichroics, spectrographs, detectors, filters, depolarizers, baffles, mounts, etc.) can be fit into place without any interference with the optical path from the sensor entrance aperture to the detectors and allow space within the instrument to insert and accurately align components. Another example is the interface between those providing the detectors and those designing the electrical system (e.g., detector taps and formats, read-out integrated circuits, ADCs). An important consideration is avoidance of electrical cross-talk between closely packaged circuits. Overall, the design team's goal is to minimize sensor size, weight, and power requirements while achieving science performance requirements. Page limitations for this chapter do not allow for a detailed or comprehensive description of all aspects of sensor design, so brief overviews of some design fundamentals and an overview of one particularly important performance parameter, SNR, are highlighted.

5.1 Basic Sensor Designs: Whiskbroom and Pushbroom

There are a variety of sensor designs that have been flown (see the appendix for some examples) or are being proposed for future missions. In general, they fall into two categories, whiskbroom and pushbroom, each having advantages and disadvantages. Figure 2 provides a representation of each. Whiskbroom sensors use a scanning mechanism that rotates a mirror (e.g., CZCS, MODIS) or telescope assembly (e.g., SeaWiFS, VIIRS) perpendicular to the orbit track at a rate that matches the spacecraft velocity such that there are no gaps between the scans. The sample rate in the scan direction is determined by the IFOV of the sensor that, in turn, is determined by the altitude and specified ground pixel size at nadir or the subsatellite point along the ground track for

tilted sensors. Scan mechanisms usually rotate a full 360° resulting in much of the scan being outside the desired ground swath, e.g., roughly 70% of the MODIS scan is not used. This has implications on the SNR as that lost sampling time (or integration time per ground pixel τ) limits the number of photons collected for each IFOV. $\tau = \text{IFOV}/(2\pi * \text{revolutions per second})$. For example, SeaWiFS at 705 km altitude and a ground resolution of 1.1 km at nadir had an IFOV of $\sim 0.09°$ and scanned 360° in 0.167 s (telescope rotation rate of 6 Hz) so the time per IFOV was about 4.2×10^{-5} s (this does not take into account the SeaWiFS TDI scheme using four detectors which increases final signal). For narrow swath sensors having high spatial resolution like the Landsat Thematic Mapper, scan mechanisms that sweep back and forth over the swath or FOV have been implemented to avoid this problem. Pushbroom designs use an array of detectors aligned in the cross-track direction, thereby avoiding a scan mechanism. The sampling rate is determined by the IFOV and the spacecraft velocity so as to achieve contiguous data in the along track direction. However, despite the substantial increase in sampling time over whiskbroom designs, other system parameters, such as detector "well depth" (maximum number of photoelectrons a detector can hold) and saturation, limit the photon count and place constraints on other design parameters such as aperture size. A limitation for pushbroom designs is the number of such subsystems that must be incorporated to achieve the desired swath for the specified spatial resolution, For example, MERIS uses five optical subsystems (cameras) and detector arrays, but has a ground swath half that of MODIS (1150 vs 2330 km). Other disadvantages include the number of detectors that must be calibrated and only partial illumination of the detector array during a lunar calibration. An advantage of pushbroom designs is the spatial resolution does not degrade with scan angle, i.e., no cosine effect, except for the increase due to the Earth's curvature.

Finally, there is the issue of optimizing the design for a specific science application, e.g., ocean color, or accommodating multiple sets of science requirements. SeaWiFS was designed specifically for ocean color and included the depolarizer, tilt mechanism, and a limited set of spectral bands. MODIS, MERIS, and GLI were multidiscipline sensors requiring additional spectral bands, but no depolarizer (incompatible with thermal IR bands) or tilt mechanism that compromised ocean data quality (especially for MODIS/Terra) and coverage. To date, SeaWiFS provided the highest quality time series and proved to be an excellent design, although it too had deficiencies due to certain performance specifications being too lax, e.g., OOB spectral response.

5.2 Design Fundamentals and Radiometric Equations

From a systems analysis perspective, the optical system of an orbital sensor can be represented by a simple lens and detector element as in Figure 3. The detector pixel and ground pixel are in the same ratio as the effective
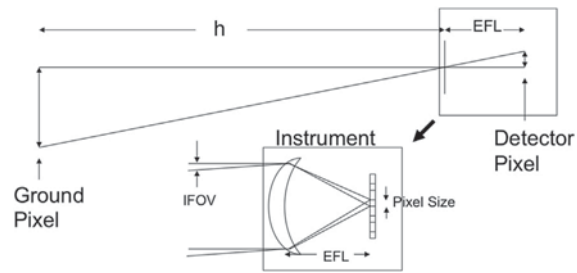
FIGURE 3 Simplified instrument optics represented by a lens aperture and effective focal length (EFL). The angle defined by detector size and EFL is geometrically similar to the angle defined by the altitude and ground pixel, and the value of the angle is IFOV.
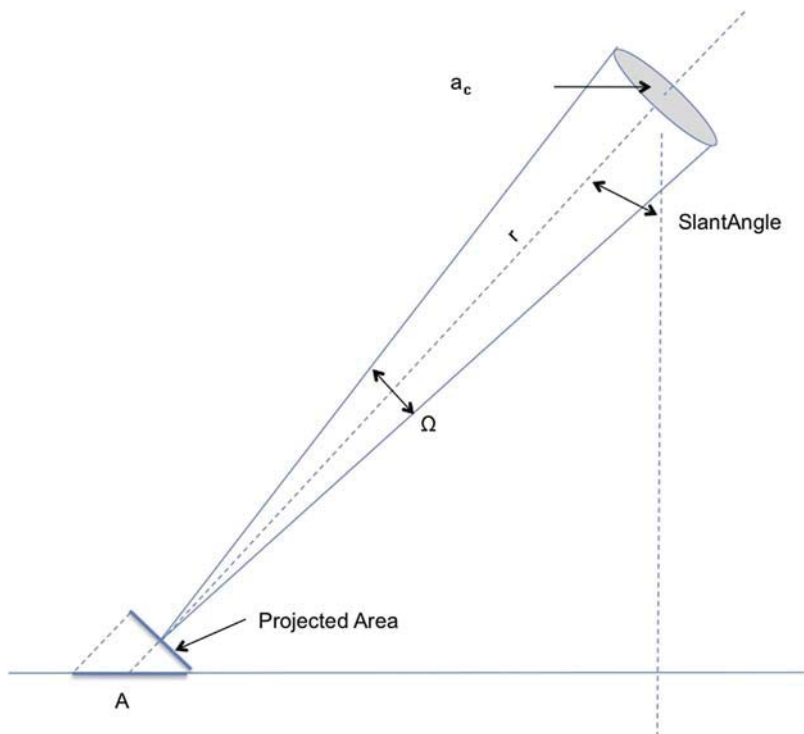
FIGURE 4 Aperture area geometry used to calculate detected power. A_c is the "clear" aperture of the instrument and is the diameter of the circular area through which light enters or is collected by the sensor.

focal length (EFL) and altitude. From Figures 4 and 5, the IFOV is the angle that encompasses the ground pixel from the satellite altitude and is calculated given the desired along-track resolution (d), tilt or slant angle (θ), and altitude (h).

FIGURE 5 Orbit geometry terms used in the text. The cross-track ground pixel has been rotated 90° for ease of viewing.

$$\text{IFOV} = \sin^{-1}\left[\frac{d\cdot\sin\left(\cos^{-1}\left(\frac{(R_e+h)\sin\theta}{R_e}\right)\right)}{r}\right] \tag{3}$$

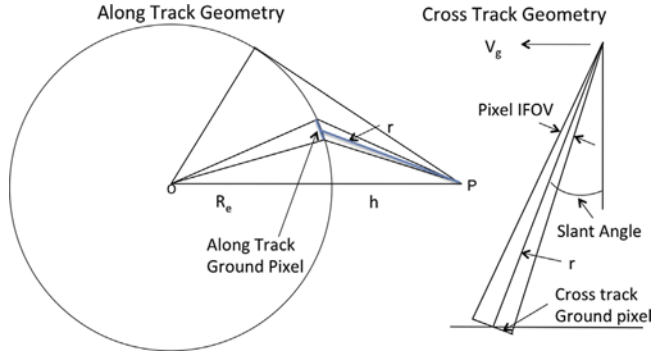or IFOV $= 2 * \tan^{-1}(a_c/2r)$. Note that for typical tilt angles of 20°, the slant range (r) is somewhat larger than $h * \tan^{-1}\theta$ due to the curvature of the earth (not shown in Figures 4 and 5 for simplicity). The corresponding cross-track resolution is simply $r *$ IFOV. Both along- and cross-track resolutions are for ground pixels on the suborbital track.

To understand how SNR influences the optical design, the geometry of the measurement must be explained (Figures 4 and 5). The solid angle of the aperture from a distance of r, is the ratio of the area of the aperture to the area of the half sphere of radius r, times the number of steradians in a hemisphere i.e., 2π [49]. Thus,

$$\Omega = \frac{\pi}{4}\left(\frac{a_c}{r}\right)^2 \tag{4}$$

Therefore, the observed power is

$$P = LA\beta\Omega \tag{5}$$

where L is the TOA radiance observed at the sensor, e.g., W/(m^2 * μm * sr) and β is the bandwidth in μm. Finally, the power actually reaching the detector surface (P_d) is simply P * E, where E the optical efficiency of the instrument.

The electronic signal output by a detector is proportional to the number of photoelectrons generated by the absorption of incident photons. The power incident multiplied by the time the power is applied, or the time before the photoelectrons are transferred out of the detector, is the energy deposited. The maximum number of photoelectrons produced is the energy deposited divided by the energy per photon. Finally, in a manner similar to the optical efficiency,

the detector produces photoelectrons with an efficiency referred to as the quantum efficiency (QE). Accounting for these factors, the final expression for the number of photoelectrons that produce the electronic signal is

$$\varepsilon = P_d \tau QE \left(\frac{\lambda}{hc} \right) \tag{6}$$

where h is Plank's constant, c is the speed of light, and τ is the dwell or integration time, i.e., the time during which photons from an IFOV are collected. The signal output from the detectors is directly proportional to ε, so ε is key to estimating SNR.

5.3 Performance Considerations

Sensor data quality depends upon a host of design factors as discussed in §4. This discussion centers on intrinsic system attributes of concern to all designs, i.e., dynamic range and sensitivity, noise, and sensor degradation due to component deterioration.

5.3.1 Dynamic Range and Sensitivity

As discussed earlier, radiance from the ocean is a small fraction of the TOA radiance measured by a satellite sensor. The range of L_{max}/L_{typ} in Table 2 is 4.75 (350 nm) to 275 (2135 nm). This huge range of light into the sensor puts a dynamic range burden on the engineering team. The problem of dynamic range is coupled to sensor sensitivity.

There are a number of strategies to deal with the large dynamic range. The obvious one is to ignore the large signal, design for clear ocean radiances, and simply let the sensor saturate when clouds are in the IFOV as was the case for some of the MODIS ocean bands. When the cloud radiance exceeds the sensor dynamic range, either the detector or the analog front-end electronics are allowed to saturate. This is rarely a satisfactory solution, as saturation by either usually leads to unacceptably long recovery time of the system as was the case with the CZCS [50]. This "bright target recovery" problem (it has many names) tends to cause uncorrectable distortions in the time decay of the output from saturation conditions. When charge-coupled device (CCD) elements or pixels saturate, charge leaks to adjacent elements and this is called "blooming" and is irreparable. One strategy to deal with a large dynamic range is to prevent the sensor from saturation by some sort of large signal overflow drain in the detector. Such structures can be designed into detectors, but frequently with an unacceptable cost in performance. The impact on performance is detector dependent, but lower efficiency and signal response nonlinearity are common issues.

Yet another strategy, and the preferable one, is to make sure neither the detector, nor the electronics, saturate. Accommodating the especially large dynamic range requirement in the red portion of the spectrum, e.g., $L_{max}/L_{typ} = 74$ (865 nm), can have a deleterious effect on sensitivity for an

ADC with 12 bits or less, and accommodating the large dynamic range can result in a signal increment per ADC count that is larger than the required sensitivity, i.e., the noise equivalent radiance (NE$\Delta L = L_{\text{typ}}$/SNR) is greater than the water-leaving radiance resolution required by the bio-optical algorithms for accurate estimation of ocean properties like chlorophyll-a. This bit resolution can be the ultimate limit on sensitivity in a sensor system where the total system noise is dominated by digitization noise (particularly true of early sensors like the CZCS). The total subsystem noise component at the digitization stage further limits sensitivity because much of the signal increment per digital count will be due to additional noise from the digitizer itself. Many of the currently orbiting sensors have 12-bit ADCs as discussed in the appendix. In recent years, a selection of 14-bit ADCs has become available for space flight. This increase in number of ADC bits promises a new generation of sensors where the total system noise, across the spectrum, is dominated by the intrinsic noise from photon counting rather than noise from the ADC, which is the desired regime for the sensor designer.

If the design choices result in loss of sensitivity in the red, given the limited digitization range and noise contributions, a solution that has been used on existing sensors is to incorporate a bilinear gain as in SeaWiFS or an automatic electronically switchable gain as in VIIRS, effectively boosting the low signal gain, and lowering the large signal gain. This effectively provides low sensitivity at large cloud radiances where the gain is low, and higher sensitivity at clear ocean radiances where the gain in high.

5.3.2 Noise

There are many types of noise that must be considered by the system designer. Some, like Johnson noise due to thermal effects in circuits, exists everywhere in the low signal analog electronics chain, irrespective of device or applied voltage. Others, like quantization noise and shot noise (related to the particle nature of light), are specific to a particular type of electronic component. Quantization noise is intrinsic to ADCs, while shot noise is counting noise, and arises as a consequence of the statistics of the Poisson distribution. The Poisson distribution describes the probabilistic nature of counting photons.

For SNR estimation, the noise contributions arise from three major conceptual subsystems: the detector, the analog front-in amplifiers, and finally the ADC. In truth, there is radiometric uncertainty in the calibration process that contributes to the overall SNR as estimated in prelaunch testing. Estimation of on-orbit uncertainty involves additional sources as well [51,52], but those sources are not considered here. The total system noise contribution from these three sources is the root mean square (RMS) of the individual contributions, assuming the sources are uncorrelated. A more thorough treatment of electronic noise and its physical origins can be found in reference texts dedicated to the subject [53]. One of the tradeoffs in defining mission science requirements is spatial resolution versus SNR. Aggregation of ground pixels

increases SNR approximately as the square root of the number of samples averaged. For example, aggregating sixteen 250-m pixels increases the 1-km aggregated sample SNR by only four, or stated another way, a 1-km pixel would have four times the SNR of sixteen aggregated 250-m pixels. Measurements or models of the individual noise contributions allow the system designer to focus on reducing, where possible, the dominant contribution in the system root sum square (RSS) noise and can result in a dramatic increase in sensor performance.

5.3.2.1 Detector Noise

There are many different types of detectors suitable for satellite ocean color sensors, the most common being silicon diodes and arrays (e.g., CCDs) for the UV-NIR and HgCdTe and InGaAs for the SWIR [54]. Some detectors and detector arrays have integral amplifiers (usually silicon) built into the device, or in the case of nonsilicon detector arrays, these amplifiers reside on the read-out integrated circuit, or ROIC, and this ROIC is electrically contacted, or bump bonded, to the detector. The contact material is usually indium because it is both somewhat physically compliant as well as electrically conductive.

In discussing detector noise, the intrinsic detector noise as well as the radiation noise that manifests itself in the detector is considered. The latter includes shot noise resulting from light being composed of discrete photons and the blackbody background radiation that can become a serious problem in the thermal region of the spectrum. Within the UV−NIR spectral range, detectors generally operate in one of two modes, photovoltaic or photoconductive. A photoconductive detector can be viewed conceptually as a variable resistance device where the resistance is a function of incident radiation having energy greater than the band-gap of the material. A photoconductive detector is essentially a *p-n* junction diode. Incident radiation with energy exceeding the band gap of the material creates electron hole pairs, increasing the carrier population. Typically, the devices operate with reverse (voltage) bias, resulting in significant increase in reverse current when the detector absorbs the incident radiation.

The total noise at the detector is specific to the type of detector (photoconductive or photovoltaic) as well as the bias voltage, the material, and a number of other factors. A comprehensive discussion of detector noise can be found in [54]. In some cases the noise can be modeled or predicted, as for many shot noise limited *p-n* devices, but in general measurements are necessary.

5.3.2.2 Read or Preamplifier Noise

Read noise is the electrical noise generated in the front-end analog electronics after the detector, though as already mentioned, it may originate on the same physical device as the actual detector. At the initial amplifier stage the signal is at its lowest, and any noise arising from the amplifier stage itself is increased along with the signal. For this reason the noise at the analog front-end is

usually dominated by the noise of the first high gain amplifier, or set of amplifiers. It is for this reason that engineers sometimes refer to the device at this first stage of amplification as the low noise amplifier, since it is here that high gain is secondary to low noise behavior when mated with detectors having low signal level outputs. Electronic noise superimposed on signal data at this early stage of amplification is bad because both the noise as well and the signal are amplified by further gain stages.

5.3.2.3 Digitization Noise

ADCs used for satellite ocean color sensors are generally successive approximation digitizers, with as many bits as possible to maximize dynamic range and maintain sensitivity, though other types of digital converters exist. An idealized ADC, where the noise is dependent only on the number of bits, does not exist since all ADCs are actually hybrid devices with an analog front-end followed by the digitization stage providing the output digital word. This analog front-end contributes to digitizer output noise, as does the following digitizing stage.

The noise performance of an ADC is summarized in the manufacturer's specification sheet, which will also specify the test conditions and the circuit configuration. Unfortunately, most commercial ADC applications relate to analog signal sampling and reconstruction, and the test parameters in the specification sheet reflect this fact. Sensor designers are interested in DC performance more than AC signal reconstruction. Satellite sensors, irrespective of the design specifics, accumulate a ground pixel signal over the integration time and digitize this essentially DC signal. The signal is usually stable, or nearly so, during the conversion. Under these conditions digitizer performance may be better than indicated by the specification sheet.

A more realistic test of the candidate ADC would be to sample a stable DC signal at the frequency desired and examine the histogram of output count values. The RMS of count values distribution is called input-referred noise or code transition noise [55] and is a good measure of how the ADC will perform in the sensor, assuming the test set-up and lay out reflects the conditions in which the converter will be used. Code-transition noise is rarely, if ever, found on the specification sheet for the device and should always be measured under realistic conditions, e.g., temperature range.

5.3.2.4 Total System Noise Reduction

Measurement of the noise associated with each component subsystem in a relevant sensor configuration is most beneficial because it highlights the component or components that dominate overall system noise. Since the individual noise terms are squared then added, a term significantly larger than others will dominate the RMS sum. This shows the system designer where to concentrate efforts to affect performance improvements. Even good estimates at an early stage can have a large payoff.

As discussed above in the context of aggregation of ground pixels, averaging can have a significant effect on reducing system noise and increasing SNR, but does come at a price compared to having larger ground pixels. However, depending on the specific design and component capabilities, signal averaging can be accomplished elsewhere in the signal chain. A common technique is to oversample at the digitization stage. Digitizing twice within the integration period and averaging the resulting digital counts will reduce the noise contribution by the square root of 2.

5.3.2.5 SNR and Noise Equivalent Radiance

SNR and NEΔL are determined from a base radiance, e.g., L_{typ}, and total system noise that is the RSS sum of all uncorrelated sensor noise sources. For early sensors, such as CZCS with 8-bit digitization, the digitization noise dominated and it was valid to consider sensor sensitivities with reference to the digitization granularity ($L_{max}/2^n$ where n is the number of bits). This is not true for sensors with digitizers having 12 bits and greater. These sensors are primarily signal limited, that is to say Poisson or shot limited.

5.3.3 End-Of-Life Performance

Sometimes overlooked in the early system design stage, lack of attention to end-of-life (EOL) performance can result in a sensor with stellar performance in its early years becoming a sensor with severely degraded performance in its latter years. Most of the issues affecting EOL are known to those organizations that routinely build flight sensors, but the comprehensiveness of EOL mitigation measures is inevitably a budget issue.

Most causes of optical sensor degradation fall into two categories: contamination and radiation damage. Radiation includes alpha and beta particles and gamma rays. Mitigating these via materials control coupled with a materials test program early in the design phase is the best way to minimize potential long term sensor degradation and is the responsibility of specialists in contamination and radiation damage. Contamination affects an optical system throughput by way of both particulates and volatile organics. Particulates are generally a concern for thermal IR systems with wavelength bands beyond 3000 nm, whereas volatile organic controls are generally more important at wavelengths shorter than 500 nm, depending on the thickness of the contaminant. However, all satellite instruments are fabricated in clean rooms. There are a number of clean room classifications. One of the more commonly used schemes, ISO 14,644−1, has nine classes categorized by the particle size and number/unit volume. Class 4 is typically used for spacecraft and sensors. Volatile carbon-based organics are sensitive to UV radiation, which is energetic enough to break organic bonds. The exact chemical mechanisms are varied and contaminant specific, but the net result is loss of transmission or reflectivity in the blue region of the spectrum.

Many transmissive optical and detector materials are susceptible to radiation damage. The mechanism is energetic defect creation in the material and can occur in both crystalline and amorphous materials. Solid-state physicists actually refer to categories of these damage sites as "color centers," because the material can visually appear to take on a color tint if enough of these damage centers are created. Lens and optical fiber materials must be carefully chosen or screened to avoid materials with damage susceptibility. Detector devices are often adversely affected by damage centers created by energetic radiation. The exact mechanisms are varied, reflecting the number of materials used as detectors, and the subject is complex. Detector damage can be mitigated by cooling and shielding which have cost and design implications. What can be said is that defect creation usually changes the electrical properties of the material, and detectors are both electrical as well as optical devices. Any flight detector must be evaluated for radiation damage effects prior to use on a space sensor. The radiation environment is determined by the altitude. The South Atlantic Anomaly is a location where the inner Van Allen belt is closest to the Earth allowing a higher flux of energetic particles. For example, Poivey et al. [56] discuss the frequency and orbital distribution of "single event upsets" for the Orbview-2 (SeaWiFS) solid state recorders.

5.4 Sensor Implementation

A space flight mission includes a number of elements, to include the ground communications, mission operations, launch (including the appropriately sized launch vehicle), data processing, space segments (e.g., the sensors and spacecraft or bus), and mission science. The science sensor is but one element of the space segment and the total mission cost cap as well as technical resource constraints in other elements may result in design compromises that limit sensor performance. This is an important point because it is easy to conceive, for example, of a sensor with data rate that is not commensurate with the capacity of the data link between spacecraft and ground station. The message here is that science requirements must be considered in a mission context, not just in the context of the sensor. Building space flight sensors and spacecraft that must survive on orbit and perform to specifications for years, without maintenance, is a challenging engineering endeavor, and the importance of quality assurance throughout the entire build process is a distinguishing feature of space flight. Quality assurance, in the context of the sensor, is the totality of the effort devoted to ensure science mission success and includes the following elements:

5.4.1 Design Controls and Margins

The design process is governed by discipline specific rules. The purpose of these rules is to prevent failure or undesirable performance degradation. These rules dictate required margins such as mechanical strength, electrical current and voltage capacity, software processing and storage, and component

temperature sensitivities to name but a few. In most cases the engineering organization maintains these rules in configuration-managed documentation.

5.4.2 Electronic Parts Selection

Parts engineering is a specialty discipline in space flight. The design engineer must stay current with changing technology in their field, both design tools as well as component technology. Knowing which specific electronic components are suitable for space flight is outside their area of expertise. The flight parts engineer's job is to monitor component vendor processes and flight part screening, keep current with bulletins regarding part restrictions and warnings, and understand parts performance in general to allow them to suggest substitutions in the electronic engineer's design, for example, when the engineer's preferred part does not exist as a flight screened or qualified version.

5.4.3 Materials Selection and Control

The materials engineer has oversight and approval authority for all materials used. The concern is primarily twofold, contamination and corrosion, although issues of material properties such as brittleness, toxicity and others are concerns. Many dissimilar metals will chemically corrode at the metallic junction over time, leading to parts failure. This includes solder joints. Many materials, especially oils, greases, plastics, and other organics will outgas in the vacuum of space, depositing films on optics and thermal control surfaces. Outgassing greases may leave a mechanism without proper lubricant, leading to increased wear and possible component failure, e.g., bearings.

5.4.4 Life Test and Component Screening

Mechanical, optical, and electronic components that are subject to degradation or failure, and for which there is little or no flight heritage or screening data, must be verified as suitable for the mission. For an electronic part, this may involve radiation testing and thermal cycling followed by electrically stressing the part to voltages, currents, or clocking speeds beyond the design limits. This screening is only valid for the lot produced during a production run where processes and materials are documented and remain constant. Parts used for flight must be from the same lot as those tested. A mechanism (e.g., scan motors and momentum compensators), or individual components of the mechanism (e.g., bearings), must be placed in a relevant thermal and vacuum environment, with the approved lubricant, and life tested. In some circumstances using rotation rates or higher duty cycles than needed for the mission may allow for an accelerated life test. In other cases the frictional properties of the lubricant will change with higher rotation rates, precluding this form of accelerated test.

5.4.5 Process Controls

Soldering and electrostatic discharge (ESD) are two examples of processes requiring special training. Soldering and ESD handling are governed by strict documented procedures, and the technicians doing this work are trained and certified, and their work and workplaces are subject to periodic quality assurance monitoring.

Plating and coating processes, whether done for optical, thermal, or other surface properties reasons, must adhere to strictly documented processes and procedures. Witness samples are usually produced along with the processed flight part to ensure, by test, that the surface modification meets standards of uniformity, surface adherence and corrosion resistance.

Printed circuit boards (PCBs) are potential failure points for electronic subsystems and quality can never be taken for granted. A PCB with dense, fine features and a large number of board layers must survive the launch vibration environment without creating mechanically weak, failure prone traces. Thermal stress caused by varying operating and survival temperatures on orbit can also cause mechanical failures. PCB fabrication is a complex process utilizing many steps and involves the use of many chemicals. Because of the many materials and chemicals used in the process, there is the possibility of process-induced corrosion. PCB quality is verified by way of PCB coupon testing. Testing involves both environmental stresses and subsequent destructive sectioning and microscopic analysis of the stressed boards.

5.4.6 Environmental Test and Performance Verification

Environmental tests are conducted on individual sensors and the fully configured spacecraft. Environmental testing at the sensor level is fundamentally a quality or workmanship battery of tests. The specific tests are designed to reveal flaws in the fabrication of the sensor or its subsystems and usually require special facilities such as large thermal-vacuum chambers that are large enough for large multi-instrument platforms such as Aqua (US), Envisat (ESA), and ADEOS (Japan). Environmental tests are not performance tests, though various levels of, or subsets of, complete performance tests are performed between or during some environmental tests. Environmental tests done with the sensor unpowered include simulation of the launch vibrational environment and sometimes load tests on the structure. The acoustic and shock tests to simulate launch conditions are also done at some level, either at the subsystem level or the space segment level with the sensor integrated to the spacecraft. Electromagnetic interference testing may also be required.

Other tests are performed with the sensor powered and operating. The thermal balance test is done with the sensor operating at select temperatures in vacuum and is designed to verify the accuracy of the thermal model for the sensor. Electromagnetic emissions and susceptibility tests are designed to

ensure that the sensor neither emits interfering radiation to other elements such as other instruments, nor is susceptible to defined levels of allowable emission from other elements. The thermal cycling test characterizes the behavior of the sensor at a variety of temperatures and places thermal stresses on the components. The temperature extremes also include sensor nonoperating survival temperatures as when the satellite goes into a "safe haven" status. Some subset of performance testing is generally performed during thermal cycling.

Various performance tests and calibrations can be performed either in vacuum or not, as appropriate. The usual approach is to perform a comprehensive performance test before environmental testing and again after environmental testing, with a limited set of performance tests done during or between environmental tests. These limited performance tests are carefully chosen to reveal anomalous behavior and to identify when in the test process the anomalous behavior occurred.

5.4.7 Reviews and Schedule

A typical satellite sensor build and test schedule is about 5 years. This assumes a specific design that conceptually, e.g., modeled, has been developed which meets the sensor performance specifications. There are a number of formal reviews held at certain milestones in the sensor development where issues may be raised. Each issue must be addressed in detail and cleared by the review panel before the instrument development can proceed. The sensor development reviews are part of a larger set of mission reviews which cover all aspects of the mission, e.g., sensor, spacecraft, launch vehicle, and ground system (including the data processing system). At NASA, the reviews have titles like the mission confirmation review, system definition review, preliminary design review, critical design review, and launch readiness review.

6. SUMMARY

Since the 1970s when the CZCS was conceived as a proof-of-concept experiment to determine if basic biological and optical properties, i.e., near surface pigment concentration and diffuse attenuation, could be estimated from space, science objectives have advanced considerably as planning for missions like PACE proceed and as outlined in [5]. Beyond hyperspectral sensors, even more advanced concepts can be envisioned such as inclusion of polarization bands as demonstrated by Loisel et al. [57] using the POLarization and Directionality of Earth Reflectance (POLDER) sensor, for example. The SGLI has polarization bands as well, but neither POLDER nor the SGLI polarization bands were designed specifically for ocean biogeochemistry applications. As the science objectives evolve and become more exacting in terms of the number of parameters or derived products and the accuracy and range of values to be quantified, sensor technology and design engineering concepts are constantly challenged to meet the associated

performance requirements. Thus, science and engineering must move forward hand-in-hand as scientists work closely with the design engineers to ensure that requirements are thoroughly documented and concisely understood by the engineers. These two groups can have very different perspectives and approaches. Advances in technology, e.g., detector systems, and optical and electronic components, required to meet future measurement requirements must be identified and funded well in advance of a flight project to ensure the technology is proven and qualified for flight prior to when a mission budget and schedule is defined. Otherwise, the mission can be at risk of cost overruns and launch delays or even cancellation. Finally, some ocean color missions are for the purpose of technology development and can accept more risk than missions providing climate research quality data to both research and operational users, e.g., MODIS. Also, these climate research missions require a comprehensive calibration and validation program as well as a robust and flexible processing system designed to provide data to operational users at short latency times while accommodating frequent data quality and algorithm tests and mission reprocessings.

ACRONYMS

ADC Analog to digital converter
CCD Charge-coupled device
CDOM Colored dissolved organic matter
Chl Chlorophyll
CZCS Coastal zone color scanner
DOP Degree of polarization
FLH Fluorescence line height
FOV Field of view
FWHM Full width half maximum
GLI Global imager
GOCI Geostationary ocean color imager
HICO Hyperspectral imager for coastal ocean
IFOV Instantaneous field of view
IOCCG International ocean colour coordinating group
IOP Inherent optical property
K(490) Diffuse attenuation at 490 nm
MERIS Medium resolution imaging spectrometer
MODIS Moderate resolution imaging spectroradiometer
NEΔL Noise equivalent radiance
NIR Near-infrared radiation
NPP Net primary production
OCI Ocean color imager
OCTS Ocean color and temperature scanner
OLCI Ocean and land colour instrument
OOB Out-of-band
PAR Photosynthetically available radiation
POC Particulate organic carbon

POLDER POLarization and directionality of earth reflectance
RSR Relative spectral response
SeaWiFS Sea-viewing wide field-of-view sensor
SGLI Second generation global imager
SNR Signal to noise ratio
STM Science traceability matrix
SWIR Shortwave infrared radiation
TDI Time-delay-integration
TOA Top of atmosphere
TSM Total suspended matter
VIIRS Visible infrared imaging radiometer suite

SYMBOLS AND DIMENSIONS

a_c Aperture (clear) diameter (millimeter (mm), centimeter (cm), meter (m))
Ω Aperture solid angle (steradians (sr))
A Area ground (square kilometers (km^2))
β Bandwidth (nanometers (nm))
m_e Earth mass (kilograms (kg))
R_e Earth radius (kilometers (km))
v_g Ground velocity (km s^{-1})
τ Integration time (seconds (s))
E Optical throughput (dimensionless)
h Orbit altitude (km)
T Orbital period (minutes (min))
ε Photoelectrons (dimensionless)
P Power (watts (W))
P_d Power (detector) (W)
QE Quantum Efficiency (dimensionless)
L Radiance (W m^{-2} μm^{-1} sr^{-1})
r Slant range (km)
V Spacecraft velocity (km/s)
θ Tilt or slant angle (degrees)

7. APPENDIX. HISTORICAL SENSORS

The sections below discuss the designs of the CZCS (US, 1978−1986), the OCTS (Japan, 1996−1997), SeaWiFS (US, 1997−2010), MODIS (US, 2000-present), and MERIS (ESA, 2002−2012). This suite of instruments includes both whiskbroom designs with various unique features (CZCS, OCTS, SeaWiFS, MODIS) and a pushbroom design (MERIS). VIIRS is a whiskbroom design which incorporates a scanning telescope like SeaWiFS and a focal plane similar to MODIS, so it is not discussed here even though it too has some unique features like aggregation zones and electronic gain switching.

7.1 CZCS and OCTS

The CZCS was a grating spectrometer design. The fore optics consisted of a rotating mirror that could be tilted in 2° increments up to ±10° (a 10° tilt results in a 20° viewing angle) to avoid sun glint. The CZCS also had another innovative element, the polarization scrambler. This component was inserted because the Rayleigh molecular scattering and surface Fresnel reflections are highly polarized, thus requiring the full Stokes parameters and sensor Mueller matrix for the atmospheric correction if no depolarization was incorporated. The sensor had six bands at 443 nm (chlorophyll-a absorption peak), 520 nm (near the spectral location least sensitive to chlorophyll-a, the "hinge point"), 550 nm (measures increased water-leaving radiance as particulate concentrations and backscatter increase), 670 nm (a secondary chlorophyll-a absorption peak), 750 nm (cloud detection), and 11.5 µm (sea surface temperature). The four visible bands had nominal bandpasses of about 20 nm. The Nimbus-7 orbit was sun-synchronous at local noon and descending (altitude = 955 km). Earth data were collected between scan angles ±39.36° with a spatial resolution of ∼800 m at nadir and a swath of 1566 km.

The sensor had four commandable gain settings (visible bands only) to compensate for the range of expected illumination conditions and, as it turns out, decreased sensitivity over time. This was necessitated by the 8-bit digitization in order to maintain the desired quantization. The SNRs ranged from about 400 (520 nm) to 140 (670 nm) for typical open ocean clear sky TOA radiances.

The sensor also had internal lamps for on-orbit calibration stability tracking, but these proved to be too unstable to be useful. The final post−mission calibration was based on global analyses of the time series using "clear-water" radiances to set the "vicarious" gain factors. Indeed, over the lifetime of the sensor, the 443 nm band sensitivity decreased by about 40% [58]. This degradation was presumably due to contamination of the scan mirror.

Being a proof-of-concept mission, some components of the system worked well and others did not. The gain on the 750 nm band was coarse so it was used only for cloud detection. Therefore, the 670 nm band was used for aerosol corrections where it was assumed that the water-leaving radiances at 670 nm were zero [25]. Ironically, this made the CZCS least reliable for measurements in turbid coastal waters.

The system polarization sensitivity was reduced by inclusion of a dual-wedge depolarizer and by positioning the folding mirror such that it compensated for the scan mirror polarization. All mirrors (scan mirror, two telescope mirrors, threefold mirrors, and the collimating mirror) had protective silver coatings. A dichroic located after the scan and two telescope mirrors separated the visible and infrared light and the depolarizer was positioned further down the optical train after the first fold mirror and the collimating mirror. Prelaunch testing showed a maximum polarization sensitivity at 443 nm of about 3% for a 10° tilt (most data was collected at a 10° mirror tilt).

Having the depolarizer located in the aft optics increases the polarization uncertainty. Assuming a DOP of 60% and a Rayleigh component of 80% of

the total radiance, the effect is roughly 1.4%. If the polarization properties of the system components stay constant, there is no issue, i.e., the Mueller matrix is known. If component reflectances and transmissions change on orbit and are sensitive to polarization, then having the depolarization wedges near the tail end of the optical path means that the system's actual polarization sensitivity is unknown, i.e., the Mueller matrix has changed.

The CZCS preamplifiers on the detectors tended to "ring" off bright targets. This electronic overshoot often persisted for tens of downscan pixels [50] and depended on how bright the up scan pixels were. No completely satisfactory algorithm for masking contaminated pixels was ever developed.

Both the CZCS and the Ocean Color and Temperature Sensor (OCTS) used a 45° "barrel roll" mirror. In this configuration the sensor aft optics were positioned either forward or aft of the mirror assembly (along the spacecraft velocity direction), and the incoming light was reflected from the Earth-viewing direction along that axis. The tilt mechanism rotated the mirror assembly within the instrument. This had the effect of changing the pixel spacing, and the total scan width, as a function of tilt angle. For example, on OCTS (±40 ° scan), the scan angle per pixel was 0.83 mrad at tilt −20° (aft), 0.72 mrad at tilt 0, and 0.58 mrad at tilt +20°. Since data are collected primarily at ± 20° degrees tilt, this resulted in a large difference in spatial resolution and coverage north and south of the tilt change (subsolar point).

On OCTS, the 45° mirror, combined with the MODIS-like focal plane design (a large 2-D array of detectors), also had the effect of rotating the effective focal plane footprint on the ground as the mirror scanned from one side to the other. As a result, the individual bands were only co-registered near nadir. As the scan angle increased from nadir, the rotation of the viewed area caused the individual bands to separate in the along-track direction. At the largest scan angles, a given location on the Earth required five consecutive scans to be viewed by all of the bands. This required substantial resampling of the bands to achieve approximate coregistration, and this process increased the noise level in the resampled data.

Both the CZCS and OCTS incorporated internal calibration lamps and OCTS also included a solar calibration capability. The OCTS digitization was 10 bits. Unlike the CZCS, OCTS did not have a depolarizer. The ADEOS-1 orbit was sun-synchronous at local 10:30 AM and descending (altitude = 800 km) and the OCTS swath was 1400 km.

7.2 SeaWiFS

SeaWiFS was a NASA data buy from Orbital Sciences Corporation who subcontracted the sensor to Hughes Santa Barbara Research Center (SBRC). The SBRC sensor design was a huge departure from the CZCS. Rather than a scan mirror, a rotating telescope with a half-angle mirror was used. The half-angle mirror rotates in the same direction and at half the speed of the telescope, thereby maintaining a constant light path into the aft optical subsystem

containing four focal planes. As a result, both sides of the half-angle mirror are in the optical path on alternating scans and slight differences in mirror reflectivity are present in the imagery, but this effect was accurately removed via the on-orbit calibration procedures. This design helped minimize polarization and protected the fore optics from contamination. VIIRS also uses a rotating telescope, but (presumably) because of the finer spatial resolution a longer focal length was required resulting in two additional telescope folding mirrors.

The SeaWiFS SNR values are 2—3 times higher than CZCS in the blue and green bands and about 6 times higher at 670 nm for the same radiances. To achieve this, each spectral band has four detectors, the signals from which are summed in a TDI scheme, i.e., each detector sees a ground pixel at a slightly different time. This requires the synchronization of the scan mechanisms and the detector read-out electronics. This feature also eliminated striping that is problematic in other designs such as MODIS and VIIRS.

Another strength of the SeaWiFS detector array or focal plane design is the bilinear gain that prevents bright pixels from saturating any band. This design was implemented to allow for a straylight correction. The original copy of SeaWiFS failed to meet straylight specifications and a number of design adjustments were made to ameliorate the problem, e.g., putting a wedge angle on the front surface of the depolarizer to "collapse" these reflections onto that of the main reflection off the mirror-coated back side [44]. A bilinear gain without electronic switching was implemented by setting the saturation of one of the four detectors at a high maximum radiance producing a "knee" in the total response as the other three detectors saturate at a lower value. Additional measures not implemented because of cost and schedule constraints included higher quality mirrors and the addition of "septums" between the detectors that would have reduced straylight even more.

The SeaWiFS sensor has eight bands in the visible (412, 443, 490, 510, 555, and 670 nm) and near-infrared (765 and 876 nm). The 412 nm band was added to improve separation of chlorophyll-a and CDOM. The 490 band was added to provide better sensitivity for chlorophyll-a estimation in coastal waters where 443 nm water-leaving radiances are small. The two NIR bands are for aerosol corrections in open ocean waters. The visible bandpasses are roughly 20 nm and the NIR bandpasses are 40 nm. The 765 nm band straddles the O_2 A-band absorption feature and requires a correction for this effect [15,16]. Also, SeaWiFS has significant OOB contamination, particularly at 555, 765 and 865 nm, due to poorly specified filter requirements [59] requiring additional corrections [60]. Improved filters to reduce OOB response should have been incorporated when the straylight issues were addressed. The SeaWiFS OOB does complicate the processing and makes comparisons with other sensors more difficult (including those used for in situ validation). The OOB was substantially higher than that of MODIS.

Like the CZCS, SeaWiFS also incorporated four commandable electronic gains and a polarization scrambler. The polarization scrambler was located behind the primary mirror (second optical component) and the sensor polarization sensitivity is estimated to be about 0.25%. Rather than internal lamps for on-orbit calibration, it had a solar diffuser with a solar diffuser cover of the same material. More importantly, the mission allowed for a monthly spacecraft pitch maneuver to scan the moon at a constant phase angle ($\sim 7°$). The solar diffuser cover was never activated to expose the solar diffuser. The diffuser cover time series provided a record for estimating changes in the SeaWiFS SNRs [51], but was not used for correcting the sensor calibration over time. Along with the daily solar calibrations, the electronic gains of each band were checked with calibration pulses. The lunar calibration established the long-term stability of the sensor at a very high accuracy [2].

The SeaWiFS orbit was initially sun-synchronous at noon, but the node drifted past 2:00 pm over the ensuing 12 years on orbit. SeaWiFS Local Area Coverage (LAC) had a spatial resolution of 1.1 km at nadir and a swath of about 2800 km ($\pm 58.3°$ scan). The SeaWiFS Global Area Coverage (GAC) subsampled the data (every fourth line and pixel for a data volume reduction of 16) and truncates the scan to $\pm 45°$ scan angles resulting in a 1500 km swath (SeaSTAR altitude = 705 km). LAC data was broadcast real time and GAC was stored on-board and downlinked to specific ground stations. The sensor tilt positions included $\pm 20°$ and $0°$, although the $0°$ position was only used for the solar and lunar calibrations. Unlike the CZCS, the whole sensor was tilted.

The SeaWiFS subsampling allows small clouds to escape detection in the GAC processing in which case straylight is uncorrected (straylight is scattered light within the instrument that contaminates measurements in adjacent pixels), thereby elevating the total radiance values. The prelaunch characterization data provided enough information for a straylight correction algorithm to be derived. This correction works well in the LAC data processing and for correcting the effects of large bright targets in the GAC.

SeaWiFS data is truncated from 12 to 10 bits on the data recorder resulting in coarser digitization, especially in the NIR bands where the SNRs are relatively low. Noise can cause jitter in the aerosol model selection amplifying the variability in visible water-leaving radiance values via the aerosol correction. Undetected clouds in the GAC data, digitization truncation, and low NIR band SNR values are thought to be the primary reasons for speckling in the SeaWiFS derived products [61].

7.3 MODIS

The design for MODIS was targeted to serve a number of research communities and, therefore, had a broader set of design requirements resulting in a much more complex sensor than CZCS and SeaWiFS. It incorporated 36 bands with wavelengths between 412 nm and 12 μm, including bands with different

spatial resolutions (1000, 500, and 250 m). Like SeaWiFS, it was built at SBRC, but about the only thing the two sensors have in common is that they both are filter radiometers, i.e., filters over the detectors for spectral separation rather than dispersive optics like gratings or prisms. Also, the MODIS data is recorded at 12 bits and provides global 1 km ocean color data (no sub-sampling). The MODIS scan is $\pm 55°$ about nadir resulting in a 2330 km swath for Aqua (1:30 pm, ascending) and Terra (10:30 am, descending) orbital altitude of 705 km.

The MODIS design uses a large rotating mirror similar to that of the CZCS and OCTS, but with no tilt. Unlike CZCS and OCTS, the mirror is not tilted relative to the nadir view, i.e., it is parallel to the local Earth tangent plane when viewing nadir. This is because the receiving optics are to the side of the scan mirror (cross-scan direction) in line with the orbit track (orthogonal to the scan). Because MODIS does not tilt, sunglint contamination is more serious than for CZCS and SeaWiFS even though the MODIS orbits are 10:30 am and 1:30 pm (the orbits have been maintained at these times) rather than noon. Having the mirror exposed does subject it to contamination, but this is tracked using the solar diffuser and solar diffuser stability monitor which provide a much more robust calibration than the SeaWiFS diffuser, but was an expensive addition to MODIS. To date, MODIS (Terra and Aqua) have experienced degradations as high as 50% (412 nm) for the ocean color bands after 12 and 10 years on orbit, respectively. The degradations are significantly different for the two mirror sides of MODIS/Terra (data is collected using both sides of the scan mirror).

MODIS can view the moon at high phase angles and spacecraft roll maneuvers are executed monthly to provide a time series at $\sim 56°$ phase angle (a partial moon). One problem with the MODIS lunar calibration is that the ocean color bands (667−869 nm) on the NIR focal plane saturate. Also, all ocean color bands saturate over clouds and those between 490 and 869 nm saturate over other bright targets such as deserts. Avoiding saturation over bright targets while maintaining high SNR and low NEΔL is one of the primary sensor engineering challenges as science objectives become more demanding.

The four MODIS focal planes (Visible, NIR, SWIR/MWIR, and LWIR) have 7−10 bands with 10−40 detectors per band. The MODIS ocean color bands are 412, 443, 531, 547, 667, 678, 748, and 869 nm. The 678 nm band is for chlorophyll-a fluorescence measurements that CZCS and SeaWiFS did not have. The 10 detectors sample 10 adjacent pixels along track allowing for a much slower scan rate (more dwell time) providing higher SNR ($\sim 1.5-3$ times higher than SeaWiFS; average of ~ 2.1 times). This is a very different strategy to achieve SNR than the SeaWiFS TDI scheme. The downside is the accurate calibration of the 10 detectors in each band. Slight differences leads to striping in the imagery.

MODIS does not have a polarization scrambler and had a prelaunch polarization sensitivity of as high as 5.4% at 412 nm. Methods for accounting for

this in the atmospheric correction have been developed [41,42], but uncertainties in the characterization and changes on orbit remain problematic, especially when other sources of error, e.g., response versus scan uncertainty (RVS), are convolved together. Indeed, for MODIS/Terra, the RVS and polarization sensitivity has changed dramatically over time, changes that cannot be accurately estimated using the on-board calibration capabilities such as the solar diffuser. A methodology for correcting these artifacts using concurrent SeaWiFS observations has been demonstrated [48].

While not designed for ocean color applications, the MODIS 1240, 1640, and 2130 nm SWIR bands (500 m) have applications for aerosol corrections over turbid water where the NIR surface reflectance is nonzero. Water absorption is orders of magnitude higher in the SWIR. The SNR values for these bands are low [62], but can be used to some degree of success [63], particularly at higher solar zenith angles (brighter illuminations).

7.4 MERIS

MERIS was an earth-observing spectrometer onboard ESA's ENVISAT satellite (altitude = 800 km, 10:00 am, descending). Remarkably, MERIS did not show significant performance degradation during its 10 years on-orbit.

The primary objective of MERIS was ocean color applications, but land and atmosphere products are an important part of the MERIS product suite as well. MERIS measured (12-bit digitization) the TOA radiances in 15 discrete bands with center wavelengths from 412 to 900 nm, with bandwidths from 3.75 to 20 nm. MERIS operated as a pushbroom scanner with five distinct cameras, pointing at five different angles in the cross-track direction, resulting in a swath width of 1150 km (FOV = 68°). This resulted in global coverage every 3 days. Each camera had its own CCD, with an imaging area of 520 lines for the spectral dimension and 740 columns in the spatial (cross-track) dimension for each CCD. Gratings are used for spectral dispersion. All MERIS bands can measure at a spatial resolution of 300 m (selected acquisitions only), but in the standard mode, 4×4 pixels are averaged to obtain an image with 1.2 km pixel size (global data set).

The calibration of MERIS was based on three solar diffusers: a white diffuser viewed frequently (diffuser-1, every 15 days), another white diffuser viewed rarely (diffuser-2, every 3 months), and a diffuser doped with Erbium. The doped diffuser was used for the spectral calibration (every 3 months), the other two to monitor (and correct) the radiometric sensitivity degradation of the instrument. The degradation of diffuser-2 was kept to a minimum by minimizing its exposure to solar radiation. The unavoidable small degradation due to the solar exposure during the rare diffuser-2 calibration events was modeled based on the degradation measured for diffuser-1 and the different solar exposure times for the two solar diffusers.

The MERIS instrument did not have a tilt capability, which leads to a relatively large loss of coverage due to glint contamination (MERIS equator crossing time was 10:00 am, so glint occurs in the eastern part of the scan) because the MERIS swath is narrow compared to MODIS for instance. The swath of the MERIS follow-on sensor, OLCI, will be shifted to the west to reduce glint contamination (this is accomplished by skewing the camera fields of view to the west side of nadir). This will increase the maximum scan angle for the western part of the scan of OLCI. Due to the pushbroom design, pixel growth for high scan angles is minimal relative to MODIS and SeaWiFS.

Each camera is an independent optical system, each with its own polarization scrambler, grating, filters (inverse filter to improve NIR performance and avoid saturation in the visible and a second-order filter to remove the second-order grating reflection), and CCD (thinned/backside illuminated for greater quantum efficiency). The transition region in the image from one camera to the next has been a challenge regarding calibration consistency, in many cases vertical lines appear in the ocean color products at the camera boundaries. The SNRs achieved vary by spectral band from 575 to 1060 for typical ocean radiances (300 m resolution [5]). The MERIS dynamic range includes typical cloud radiances without having to use different gain states.

REFERENCES

[1] G.L. Clarke, G.C. Ewing, C.J. Lorenzen, Spectra of backscattered light from sea obtained from aircraft as a measure of chlorophyll concentration, Science 16 (1970) 1119−1121.

[2] R.E. Eplee Jr., G. Meister, F.S. Patt, B.A. Franz, S.W. Bailey, C.R. McClain, The on-orbit calibration of SeaWiFS, Appl. Opt. 51 (36) (2013a) 8702−8730.

[3] C.R. McClain, Satellite remote sensing: ocean color, in: Encyclopedia of Ocean Sciences, Elsevier Ltd., London, 2009a, pp. 4403−4416.

[4] C.R. McClain, A decade of satellite ocean color observations, Annu. Rev. Marine Sci. 1 (2009b) 19−42.

[5] IOCCG, Mission requirements for future ocean-colour sensors, in: C.R. McClain, G. Meister (Eds.), Reports of the International Ocean-Colour Coordinating Group, Number 13, IOCCG, Dartmouth, Canada, 2012, 98 pp.

[6] R.M. Pope, E.S. Fry, Absorption spectrum (380-700 nm) of pure water. II. Integrating cavity measurements, Appl. Opt. 36 (33) (1997) 8710−8723.

[7] R. Bidigare, M.E. Ondrusek, J.H. Morrow, D.A. Kiefer, In vivo absorption properties of algal pigments, Proc. SPIE, Ocean Opt. X 1302 (1990) 290−302, http://dx.doi.org/10.1117/12.21451.

[8] H.R. Gordon, M. Wang, Retrieval of water-leaving radiance and aerosol optical thickness over the oceans with SeaWiFS: a preliminary algorithm, Appl. Opt. 33 (3) (1994) 443−452.

[9] M. Wang, Remote sensing of the ocean contributions from ultraviolet to near-infrared using the shortwave infrared bands: simulations, Appl. Opt. 46 (2007) 1535−1547.

[10] S.W. Bailey, B.A. Franz, P.J. Werdell, Estimation of near-infrared water-leaving reflectance for satellite ocean color data processing, Opt. Express 18 (7) (2010) 7521−7527.

[11] S. Alvain, C. Moulin, Y. Dandonneau, F.M. Bréon, Remote sensing of phytoplankton groups in case 1 waters from global SeaWiFS imagery, Deep-sea Res. 52 (2005) 1989−2004.
[12] Z.-P. Lee, K. Carder, R. Arnone, M.-X. He, Determination of primary spectral bands for remote sensing of aquatic environments, Sensors 7 (2007) 3428−3441.
[13] P.J. Werdell, et al., Generalized ocean color inversion model for retrieving Marine inherent optical properties, Appl. Opt. 52 (10) (2013) 2019−2037.
[14] Z. Ahmad, C.R. McClain, J.R. Herman, B.A. Franz, E.J. Kwaitkowska, W.D. Robinson, E.J. Bucsela, M. Tzortziou, Atmospheric correction of NO_2 absorption in retrieving water-leaving reflectances from the SeaWiFS and MODIS measurements, Appl. Opt. 46 (26) (2007) 6504−6512.
[15] K. Ding, H.R. Gordon, Analysis of the influence of O_2 A-band absorption on atmospheric correction of ocean-color imagery, Appl. Opt. 34 (12) (1995) 2068−2080.
[16] M. Wang, Validation study of the SeaWiFS oxygen a-band absorption correction: comparing the retrieved cloud optical thicknesses from SeaWiFS measurements, Appl. Opt. 38 (6) (1999) 937−944.
[17] P. Dubuisson, R. Frouin, D. Dessailly, L. Duforêt, J.-F. Léon, K. Voss, D. Antoine, Estimating the altitude of aerosol plumes over the ocean from reflectance ratio measurements in the O_2 A-band, Remote Sens. Environ. 113 (2009) 1899−1911.
[18] B.-C. Gao, Y.J. Kaufman, W. Han, W.J. Wiscombe, Correction of thin cirrus path radiances in the 0.4−1.0 μm Spectral range using the sensitive 1.375 μm Cirrus detecting channel, J. Geophys. Res. 103 (D24) (1998) 32,169−32,176.
[19] B.-C. Gao, P. Yang, W. Han, R.-R. Li, W.J. Wiscombe, An algorithm using visible and 1.38-μm channels to retrieve cirrus cloud reflectances from aircraft and satellite data, IEEE Trans. Geosci. Remote Sens. 40 (8) (2002) 1659−1668.
[20] H.R. Gordon, T. Zhang, F. He, K. Ding, Effects of stratospheric aerosols and thin cirrus clouds on the atmospheric correction of ocean color imagery: simulations, Appl. Opt. 36 (3) (1997a) 682−697.
[21] G. Meister, B.A. Franz, C.R. McClain, Influence of Thin Cirrus Clouds on Ocean Color Products, in: Ocean Remote Sensing: Methods and Applications, vol. 7459, SPIE, San Diego, 2009, 12 pp. http://dx.doi.org/10.1117/12.827272.
[22] IOCCG, Ocean-colour observations from a geostationary orbit, in: D. Antoine (Ed.), Reports of the International Ocean-colour Coordinating Group, Number 12, IOCCG, Dartmouth, Canada, 2012b, 103 pp.
[23] G. Meister, C. McClain, Z. Ahmad, S.W. Bailey, R.A. Barnes, S. Brown, G.E. Eplee, B. Franz, A. Holmes, W.B. Monosmith, F.S. Patt, R.P. Stumpf, K.R. Turpie, P.J. Werdell, Requirements for an Advanced Ocean Radiometer, NASA T/M-2011-215883, NASA Goddard Space Flight Center, Greenbelt, Maryland, 2011, 37 pp.
[24] IOCCG, Minimum requirements for an operational ocean-Colour sensor for the open ocean, in: A. Morel (Ed.), Reports of the International Ocean-colour Coordinating Group, Number 1, IOCCG, Dartmouth, Canada, 1998, 46 pp.
[25] H.R. Gordon, D.K. Clark, J.W. Brown, O.B. Brown, R.H. Evans, W.W. Broenkow, Phytoplankton pigment concentrations in the Middle Atlantic Bight: comparison of ship determinations and CZCS estimates, Appl. Opt. 22 (1) (1983) 20−36.
[26] J.E. O'Reilly, S. Maritorena, B.G. Mitchell, D.A. Siegel, K.L. Carder, S.A. Garver, M. Kahru, C. McClain, Ocean color chlorophyll algorithms for SeaWiFS, J. Geophys. Res. 103 (C11) (1998) 24937−24953.
[27] S.W. Bailey, P.J. Werdell, A multi-sensor approach for the on-orbit validation of ocean color satellite data products, Remote Sens. Environ. 106 (2006) 12−23.

[28] IOCCG, Remote sensing of inherent optical properties: fundamentals, tests of algorithms and applications, in: Z.P. Lee (Ed.), Reports of the International Ocean-colour Coordinating Group, Number 6, IOCCG, Dartmouth, Canada, 2006, 126 pp.

[29] PACE, Pre-aerosol, Clouds, and Ocean Ecosystem, 2012 (PACE) Mission Science Definition Team Report, 274 pp. http://decadal.gsfc.nasa.gov/PACE.html

[30] G. Thuiller, M. Herse, D. Labs, T. Foujols, W. Peetermans, D. Gillotay, P.C. Simon, H. Mandel, The solar spectral irradiance from 200 to 2400 nm as measured by the SOLSPE and EURECA Missions, Solar Phys. 214 (2003) 1−22.

[31] X. Xiaoxiong, N. Che, W.L. Barnes, Terra MODIS on-orbit spectral characterization and performance, IEEE Trans. Geosci. Remote Sens. 44 (8) (2006) 2198−2206.

[32] S. Delwart, R. Preusker, L. Bourg, R. Santer, D. Ramon, J. Fischer, MERIS in-flight spectral calibration, Int. J. Remote Sens. 28 (3−4) (2007) 479−496.

[33] IOCCG, Atmospheric correction for remotely-sensed ocean-colour products, in: M. Wang (Ed.), Reports of International Ocean-color Coordinating Group, Number 10, IOCCG, Dartmouth, Canada, 2010, 78 pp.

[34] W.W. Gregg, F.P. Patt, Assessment of tilt capability for spaceborne global ocean color sensors, IEEE Trans. Geosci. Remote Sens. 32 (4) (1994) 866−877.

[35] E.J. Kwiatkowska, C.R. McClain, Capabilities for extracting phytoplankton diurnal variability using ocean color data from SeaWiFS, MODIS-Terra, and MODIS-Aqua, Int. J. Remote Sens 30 (24) (2009) 6441−6459.

[36] IOCCG, In-flight calibration of ocean-colour sensors, in: R. Frouin, (Ed.), Reports of International Ocean-Color Coordinating Group, Number 15, Dartmouth, Canada, 106 pp., 2013.

[37] B.A. Franz, S.W. Bailey, P.J. Werdell, C.R. McClain, Sensor-independent approach to the vicarious calibration of satellite ocean color radiometry, Appl. Opt. 46 (22) (2007) 5068−5082.

[38] F.E. Nicodemus, J.C. Richmonds, J.J. Hsia, I.W. Ginsberg, T. Lamperis, Geometric Considerations and Nomenclature for Reflectance, vol. 160, US Department of Commerce, National Bureau of Standards, Monogram, 1977, 67 pp.

[39] G. Meister, J. Sun, R. Eplee, F. Patt, X. Xiong, C. McClain, Sun beta angle residuals in solar diffuser measurements of the MODIS ocean bands, Earth Observing Systems XIII, SPIE, Vol. 7081 (2008) 12. http://dx.doi.org/10.1117/12.796291.

[40] S. Maritorena, D.A. Siegel, A. Peterson, Optimization of a semi-analytical ocean color model for global scale applications, Appl. Opt. 41 (15) (2002) 2705−2714.

[41] H.R. Gordon, T. Du, T. Zhang, Atmospheric correction of ocean color sensors: analysis of the effects of residual instrument polarization sensitivity, Appl. Opt. 36 (1997b) 6938−6948.

[42] G. Meister, E.J. Kwiatkowska, B.A. Franz, F.S. Patt, G.C. Feldmam, C.R. McClain, Moderate-resolution imaging spectroradiometer ocean color polarization correction, Appl. Opt. 44 (26) (2005) 5524−5535.

[43] G. Meister, C.R. McClain, Point-spread function of the ocean color bands of the moderate resolution imaging spectrometer on aqua, Appl. Opt. 49 (32) (2010) 6276−6285.

[44] R.A. Barnes, A.W. Holmes, W.E. Esaias, in: S.B. Hooker, E.R. Firestone, J.G. Acker (Eds.), Stray; Light in the SeaWiFS Radiometer, NASA Tech. Memo. 104566, vol. 31, NASA Goddard Space Flight Center, Greenbelt, Maryland, 1995, 76 pp.

[45] S. Delwart, L. Bourg, Radiometric calibration of MERIS, Proc. SPIE. 7474 (2009) 12. http://dx.doi.org/10.1117/12.567989.

[46] J. Sun, X. Xiong, W.L. Barnes, MODIS solar diffuser stability monitor sun view modeling, IEEE Trans. Geosci. Remote Sens. 43 (8) (2005) 1845−1854.

[47] R.E. Eplee, K.R. Turpie, G. Meister, F.S. Patt, G.F. Fireman, B.A. Franz, C.R. McClain Jr., A Synthesis of VIIRS Solar and Lunar Calibrations, in: Observing Systems XVIII, vol. 8866, Proc. SPIE, San Diego, 2013b, 21 pp. http://dx.doi.org/10.1117/12.2024069.

[48] E.J. Kwiatkowska, B.A. Franz, G. Meister, C.R. McClain, X. Xiong, Cross-calibration of ocean color bands from moderate resolution imaging spectroradiometer on terra platform, Appl. Opt. 47 (36) (2008) 6796−6810.

[49] J. Wertz, W. Larson, Space Mission Design and Analysis, Kluwer Academic Publishers, Dordrecht, Netherlands, 1991, 811 pp.

[50] J.L. Mueller, Nimbus-7 CZCS: electronic overshoot due to cloud reflectance, Appl. Opt. 27 (3) (1988) 438−440.

[51] R.E. Eplee, F.S. Patt, R.A. Barnes, C.R. McClain, SeaWiFS long-term solar diffuser reflectance and sensor signal-to-noise analyses, Appl. Opt. 46 (5) (2007) 762−773.

[52] C. Hu, L. Feng, Z. Lee, C. Davis, A. Mannino, C. McClain, B. Franz, Dynamic range and sensitivity requirements of satellite ocean color sensors: learning from the past, Appl. Opt. 51 (25) (2012) 6045−6062.

[53] G. Vasilescu, Electronic Noise and Interfering Signals, Springer-Verlag, Berlin, 2005, 709 pp.

[54] A. Rogalski, Infrared Detectors, second ed., CRC Press, Boca Raton, Florida, 2011, 876 pp.

[55] W. Kester, ADC noise: the good, the bad and the ugly. Is no noise good noise? Analog Dialog 40 (2) (2006) 1−5.

[56] C. Poivey, J.L. Barth, K.A. LaBel, G. Gee, H. Safren, In-flight observations of long-term single-event effect (SEE) performance on Orbview-2 solid state recorders (SSR), in: Radiation Effects Data Workshop 2003, IEEE, vol. 102(107), 2003, pp. 21−25. http://dx.doi.org/10.1109/REDW, 1281357, 2003.

[57] H. Loisel, L. Duforet, D. Dessailly, M. Chami, P. Dubuisson, Investigation of the variations in water leaving polarized reflectance from the POLDER satellite data over two biogeochemical contrasted oceanic areas, Opt. Exp. 16 (17) (2008) 12905−12918.

[58] R.H. Evans, H.R. Gordon, CZCS "System calibration": a retrospective examination, J. Geophys. Res. 99 (C4) (1994) 7293−7307.

[59] R.A. Barnes, A.W. Holmes, W.L. Barnes, W.E. Esaias, C.R. McClain, in: S.B. Hooker, E.R. Firestone, J.G. Acker (Eds.), SeaWiFS Prelaunch Radiometric Calibration and Spectral Characterization, NASA Tech. Memo. 104566, vol. 23, NASA Goddard Space Flight Center, Greenbelt, Maryland, 1994, 55 pp.

[60] H.R. Gordon, Remote sensing of ocean color: a methodology of dealing with broad spectral bands and significant out-of-band response, Appl. Opt. 34 (1995) 8363−8374.

[61] C. Hu, K.L. Carder, F.E. Muller-Karger, How precise are SeaWiFS ocean color estimates? implications of digitization-noise errors, Remote Sens. Environ. 76 (2) (2001) 239−249.

[62] P.J. Werdell, B.A. Franz, S.W. Bailey, Evaluation of shortwave infrared atmospheric correction for ocean color remote sensing in Chesapeake Bay, Remote Sens. Environ. 114 (2010) 2238−2247.

[63] M. Wang, W. Shi, Estimation of ocean contribution at MODIS near-infrared wavelengths along the East Coast of the U.S.: two case studies, Geophys. Res. Lett. 32 (2005) L13606. http://dx.doi.org/10.1029/2005GL022917, 5 pp.